Ana Maria Franco
Aveiro Marote

Os efeitos dos polímeros piezoeléctricos na diferenciação neuronal

The effects of piezoelectric polymers on neuronal differentiation

Ana Maria Franco Aveiro Marote

Os efeitos dos polímeros piezoeléctricos na diferenciação neuronal

The effects of piezoelectric polymers on neuronal differentiation

Dissertação apresentada à Universidade de Aveiro para cumprimento dos requisitos necessários à obtenção do grau de Mestre em Biomedicina Molecular, realizada sob a orientação científica da Professora Doutora Odete da Cruz e Silva, Professora Auxiliar com agregação da Secção Autónoma de Ciências da Saúde da Universidade de Aveiro e co-orientação da Professora Doutora Sandra Vieira, Professora Auxiliar convidada da Secção Autónoma de Ciências da Saúde.

Dedico este trabalho à minha família, por todo o apoio e carinho, apesar da distância.

o júri
presidente

Professora Doutora Ana Gabriela da Silva Cavaleiro Henriques
Prof. Auxiliar Convidada, Secção Autónoma de Ciências da Saúde,
Universidade de Aveiro

Professora Doutora Odete Abreu Beirão da Cruz e Silva
Prof. Auxiliar com agregação, Secção Autónoma de Ciências da Saúde,
Universidade de Aveiro

Professora Doutora Sandra Isabel Moreira Pinto Vieira
Prof. Auxiliar Convidada, Secção Autónoma de Ciências da Saúde,
Universidade de Aveiro

Professora Doutora Maria Helena Figueira Vaz Fernandes
Professora Associada, Departamento de engenharia de materiais e cerâmica,
Universidade de Aveiro

agradecimentos

À professora Sandra Vieira, por desde sempre inspirar o meu interesse pela ciência e por todo o seu apoio.

À professora Odete Cruz e Silva pela orientação desta dissertação e pela oportunidade de realizar este trabalho no laboratório de neurociências do CBC.

À Nathalie, pela colaboração neste projeto e por tudo o que me ensinou.

A toda a minha família, em especial aos meus pais e irmãos, por acreditarem em mim e por toda a força que me deram nesta etapa da minha vida.

À minha prima Angelina, pela amizade.

Ao Pedro, por estar sempre ao meu lado.

Aos 3R's: Rocha, Regina e Roberto por toda a paciência que tiveram comigo e pelo bom ambiente de trabalho que proporcionaram ao longo deste ano.

À Luísa e à Catarina, pela partilha dos bons e maus momentos. À Patrícia, pelo companheirismo e amizade. Ao João e à Sónia.

A todos os meus amigos, em especial à Nádia, Juliana, Marta, Andreia, Mega e Emanuel pelos bons momentos de convívio que ajudaram a ultrapassar as adversidades do trabalho.

A todos os meus colegas do laboratório de Neurociências, em especial à Mariana por todos os seus sábios conselhos. A todos os membros do CBC.

Ao doutor Rui Vitorino, pela valiosa ajuda na espectrometria de massa.

À FCT por ter apoiado a realização deste trabalho.

palavras-chave   Diferenciação, neurónios, citoesqueleto, neurites, PLLA,filmes, nanofibras, polarização.

resumo   O crescimento de neurites é crucial para o desenvolvimento neuronal, bem como para a plasticidade e reparação na fase adulta. Após uma lesão neuronal, o sucesso da reparação é determinando pelas propriedades plásticas constitutivas dos neurónios afetados e pelo seu potencial de regeneração, que é influenciado por sinais externos físicos (ex.: cicatriz glial) e químicos (ex.: moléculas inibitórias). Recentemente, o desenvolvimento de materiais à nano-escala, que interagem com os sistemas biológicos a nível molecular, prometem revolucionar o tratamento das lesões do Sistema Nervoso Central e Periférico. Os scaffolds de nanomateriais podem suportar e promover o crescimento de neurites e consequentemente, intervir nas complexas interações moleculares que ocorrem a após o dano neuronal, entre as células e o seu ambiente extracelular. Vários estudos têm demonstrado que os materiais piezoeléctricos, que geram carga elétrica em resposta ao *stress* mecânico, podem ser usados para a preparação de *scaffolds* eletricamente carregados que devem influenciar o comportamento celular.

Este estudo centrou-se nos efeitos dos materiais baseados em PLLA (ácido poli (L – láctico)) sob a forma de filmes, nanofibras orientadas aleatória e alinhadamente, e da sua polarização, na diferenciação neuronal.

A linha celular de neuroblastoma (SH-SY5Y) foi utilizada para avaliar o efeito dos materiais-baseados em PLLA na adesão, viabilidade, morfologia celular, bem como na diferenciação tipo-neuronal. A análise proteómica baseada em espectrometria de massa das células cultivadas em nanofibras de PLLA foi também efetuada. Os neurónios corticais embriónicos foram seguidamente utilizados para avaliar os efeitos das nanofibras de PLLA alinhadas e da sua polarização no crescimento de neurites.

Nesta análise, descobrimos que os materiais de PLLA parecem inibir parcialmente a proliferação celular, enquanto promovem a diferenciação, alterando os níveis das proteínas que intervêm nestes processos. Ocorrem alterações significativas do citoesqueleto, particularmente ao nível do citoesqueleto de actina, que não induzem mas parecem potenciar o crescimento de neurites sob exposição a um sinal extracelular como o ácido retinóico. Este efeito parece ser particularmente evidente para as nanofibras de PLLA alinhadas, que induzem efeitos intermédios na restruturação do citoesqueleto. Em geral, a polarização das amostras de PLLA tem efeitos benéficos na proliferação celular e potencia o crescimento de neurites, particularmente nos neurónios.

Acreditamos que as nanofibras de PLLA alinhadas serão um bom *scaffold* para regeneração neuronal, uma vez que mimetiza o ambiente mecânico natural das células. Contudo, futuras experiências *in vitro* e *in vivo* são necessárias para comprovar a eficácia deste potencial *scaffold*.

keywords

Differentiation, neurons, cytoskeleton, neurites, PLLA, films, nanofibers, polarization

abstract

Neuritic growth is crucial for neural development, as well as for adaptation and repair in adulthood. Upon neuronal injury, the successful neuritic regrowth is determined by the constitutive plastic properties of neurons and by their regenerative potential, which is influenced by physical (e.g. glial scar) and chemical (e.g. inhibitory molecules) extrinsic cues. Recently, the development of nanometer-scale materials, which can interact with biological systems at a molecular level, provide hope to revolutionize the treatment of central and peripheral nervous system injuries. Nanomaterial scaffolds can support and promote neuritic outgrowth and consequently, take part in the complex molecular interactions between cells and their extracellular environment after neuronal injury. Several studies have shown that piezoelectric materials, which generate electrical charge in response to mechanical strain, may be used to prepare bioactive electrically charged scaffolds that may influence cell behavior.

This study focused on the effects of PLLA (poly-L-lactic acid) – based materials in the form of films, random and aligned nanofibers, and of their polarization, on neuronal-like and neuronal differentiation.

The neuroblastoma SH-SY5Y cell line was used to evaluate the effect of PLLA – based materials on cellular adhesion, viability, morphology and neuron-like differentiation. Mass spectrometry-based proteomic analysis of cells grown on PLLA nanofibers was also conducted. Primary embryonic cortical neurons were further used to evaluate the effect of PLLA aligned nanofibers and their polarization on neuritic outgrowth.

In this analysis, we found that PLLA materials seem to partially inhibit cell proliferation, while promoting neuronal differentiation, altering the levels of proteins that intervene in these processes. Dramatic cytoskeleton remodeling occurs, particularly at the actin cytoskeleton level, which does not induce but may potentiate neuritic outgrowth upon exposure to an extracellular cue, such as Retinoic Acid. This effect seems to be particularly evident for PLLA aligned nanofibers, which induce intermediate effects in the cytoskeleton remodeling. In general, polarization of the PLLA polymers has beneficial effects on cell proliferation and potentiates the neuritic outgrowth, particularly in neurons.

We believe that polarized PLLA aligned nanofibers would be a good scaffold for neuronal regeneration, since it mimics the natural mechanical cell environment and enhances neuritic outgrowth. However, further *in vitro* and *in vivo* investigations are required to prove the efficacy of this potential scaffold.

Index

Abbreviations

ABPs	Actin-binding proteins
BDNF	Brain-derived neurotrophic factor
BSA	Bovine serum albumin
Ca^{2+}	Calcium
CaMKII	Calmodulin-dependent protein kinase II
Cdc 42	Cell division control protein 42
cGMP	Cyclic guanosine monophosphate
CNS	Central nervous system
CRIB	Cdc42/Rac interactive binding region motif
CSPGs	Chondroitin Sulfate Proteoglycans
DAPI	4',6-diamidino-2-phenylindole
DNA	Deoxyribonucleic acid
ECL	Enhanced chemiluminescence
ECM	Extracellular matrix
ER	Endoplasmic reticulum
ERK	Extracellular signal-regulated kinases
F-actin	Filamentous actin
FAK	Focal adhesion kinase
FBS	Fetal bovine serum
G-actin	Globular actin
GAP-43	Growth-associated protein-43
GDP	Guanosine diphosphate
GSK-3	Glycogen synthase kinase 3
GTP	Guanosine triphosphate
HEPES	4-(2-hydroxyethyl)-1-piperazineethanesulfonic acid

HSPGs	Heparin sulfate proteoglycans
IgCAMs	Immunoglobulin superfamily cell adhesion molecules
IRSp53	Insulin receptor substrate protein of 53 kDa
JKN	c-Jun N-terminal kinase
K^+	Potassium
kDa	Kilodalton
LKB	Serine/threonine kinase 11
MAPs	Microtubule-associated proteins
MAP1B	Microtubule-associated protein 1B
MARK	Microtubule affinity-regulated kinase
MEK	Mitogen-activated protein kinase/extracellular signal-regulated kinase
MFs	Microfilaments
MLC	Myosin light chain
mRNA	Messenger Ribonucleic acid
MTs	Microtubules
NFs	Neurofilaments
NgCAM	Neuron-glia cell adhesion molecule
NGF	Nerve growth factor
NT	Neurotrophin
PAK1	P21-Activated kinase 1
PC12 cells	Pheochromocytoma cell line 12
PI3-kinase	Phosphatidylinositol-3 kinase
PIP3	Phosphatidylinositol (3,4,5)-triphosphate
PKA	cAMP-dependent protein kinase
PKC	Protein kinase C
PLLA	Poly-L-lactic acid

PNS   Peripheral Nervous System

PTEN   Phosphatase and tensin homolog deleted on chromosome 10

RA   Retinoic acid

Rac 1   Ras-related C3 botulinum toxin substrate 1

Rho   Ras homolog

ROCK   Rho-associated kinase

RT   Room temperature

SAD   Also known as BRKS2 - BR serine/threonine kinase 2

SDS   Sodium dodecylsulfate

Sema 3A   Semaphorin 3A

sGC   Soluble Guanylate Cyclase

SH-SY5Y   Human neuroblastoma cell line -- differentiated

TBS   Tris-Buffered Saline

TBS-T   Tris-Buffered Saline Tween

TGFβ   Transforming growth factor beta

Trk   Tyrosine kinases

VASP   Vasodilator-stimulated phosphoprotein

VPS   Vacuolar protein sorting

WASP   Wiskott-Aldrich Syndrome Protein

WAVE   WASP-family verprolin-homologous protein

WB   Western blotting

1. Introduction

The human nervous system is composed of more than 10 billion neurons that form circuits in order to control and integrate the functional activities of the organs and organ systems and to underlie all our thoughts, emotions, dreams and memories. Anatomically, the nervous system can be divided into central and peripheral components. The Central Nervous System (CNS) includes the brain and the spinal cord, whereas the Peripheral Nervous System (PNS) can be divided into sensory and motor portions, the later comprising the somatic motor division and the autonomic motor division [1-3].

1.1. Neurons and Glial cells

The nerve tissue comprises two categories of cells: *neurons* that are the structural and functional unit of the nervous system, and *supporting cells - neuroglia*, that supply both structural and physiological support to neurons and also respond to injury or disease [1, 4]. Neurons and glia differ in their morphology, distribution of organelles within the cell, and in cytoskeletal composition [2].

Neurons exhibit a complex, dynamic and highly polarized morphology that is characterized by a single long axon and several short dendrites (figure 1) [5]. This morphology is essential for their specialized function in communication, which comprises receiving stimuli from other cells, processing those stimuli and conducting electrical impulses over long distances to other cells [2].

The neuron is composed by the cell body, dendrites and the axon that are structural and functionally distinct from each other. Together dendrites and the axon are known as the neurites or neuronal processes. The cell body is described as a dilated region, with a large euchromatic nucleus containing a prominent nucleolus. The perinuclear cytoplasm contains an abundant rough surfaced endoplasmic reticulum (rER), free ribosomes, Nissl bodies (that represent an accumulation of many rER), numerous mitochondria, a large perinuclear Golgi apparatus, lysosomes, transport vesicles and inclusions. This composition is required to maintain the high level of protein synthesis to replace enzymes, neurotransmitter substances, membrane components, and other complex molecules, which are transported to distant locations within a neuron - axonal transport [1]. Dendrites arise from the neuronal cell body, branching into dendritic processes, which are the primary target for synaptic input from other neurons [2]. Dendrites have a greater diameter than axons and possess a similar content of the perinuclear

cytoplasm of the cell [1]. Furthermore, these structures contain mRNAs and many ribosomes free or bound to the membrane, which suggest an efficient translational activity [6]. The <u>axon</u> is a unique extension from the neuronal cell body, specialized in conducting the action potential, with a length that can vary between a few hundred micrometers (μm) and a meter depending on the type of neuron [2]. The axon hillock usually lacks large cytoplasmic organelles but contains microtubules, neurofilaments, mitochondria, and vesicles. The axon terminal contains synaptic vesicles, neurotransmitter transporters and vesicle-associated proteins [5]. Recent studies also indicate that in some large axon terminals local protein synthesis may occur, since it contains polyribosomes with complete translational machinery for protein synthesis [7, 8]. These discrete areas are called periaxoplasmic plaques and possess biochemical and molecular characteristics of active protein synthesis [1].
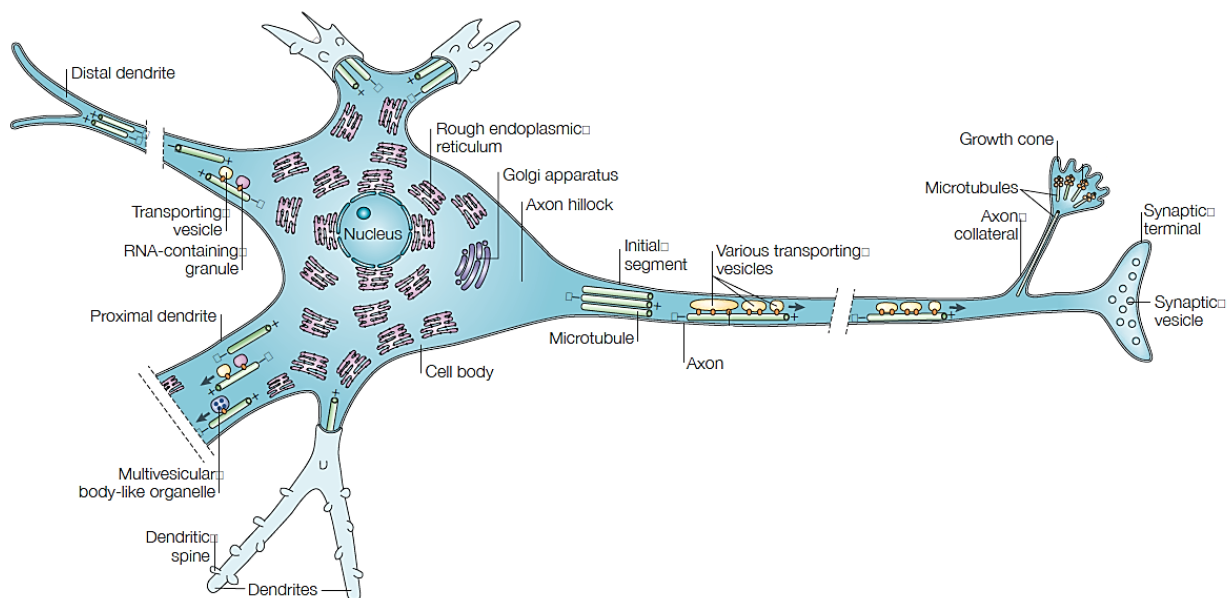
Figure 1 - Diagram of a typical neuron extending several dendrites (left) and a single thin axon (right) from the cell body. Rough endoplasmic reticula are abundant in most parts of the cell body, except in the axon hillock. Dendrites contain some rough endoplasmic reticula. Microtubules have mixed polarity in proximal dendrites, but are unipolar in distal dendrites, with the plus end pointing away from the cell body. Adapted from [9]

Neuroglial cells do not participate directly in synaptic interaction or electrical signaling; however they provide physical protection for neurons and may aid or prevent recovery from neural injury [1, 2, 4]. There are distinct types of glial cells in the human nervous system specific for the PNS and CNS, which are specialized into different functions (see table 1).

Table 1 – Types of glial cells in the PNS and CNS and their functions.

Peripheral neuroglia	Schwann cells	Produce a lipid-rich layer - myelin sheath - that isolates the axon and ensures the rapid communication of nerve impulses; Aid in cleaning up PNS debris and guide the regrowth of PNS axon.
	Satellite cells	Small cuboidal cells that surround the neuronal cell bodies of ganglia; Help to establish and maintain a controlled microenvironment; Provide electrical insulation as well as a pathway for metabolic exchanges.
Central neuroglia	Astrocytes	Star-like appearance (presence of elaborated processes); *Protoplasmic astrocytes* (gray matter; numerous, short, branching cytoplasmic processes) vs. *Fibrous astrocytes* (white matter, with fewer processes); Maintain tight junctions of the capillaries that form the blood–brain barrier; Cover the nodes of Ranvier and synapses; Confine neurotransmitters to the synaptic cleft and remove excess of neurotransmitters by pinocytosis; Scaffolds for migrating neurons during brain development; Buffer the K^+ concentration in the extracellular space of the brain.
	Oligodendrocytes	Small cells active in the formation and maintenance of myelin in the CNS, which serves to enhance axonal transmission; Contain few processes that myelinate one axon or several nearby axons distant from the oligodendrocyte cell body.
	Microglia	Resident immune system phagocytic cells that remove cellular debris from sites of injury or normal cell turnover; Secrete signaling molecules that modulate local inflammation and influence cell survival or death.
	Ependymal cells	Form a single layer of cuboidal-to-columnar cells that have the morphologic and physiologic characteristics of fluid-transporting cells.

Neuronal cytoskeletal elements

The cytoskeleton provides structure to cells and also serves many fundamental physiological functions, being especially important in neuronal differentiation and regeneration [10]. Neuronal cytoskeleton consists of three distinct structural complexes with different properties: microtubules (MTs), neurofilaments (NFs) and microfilaments (MFs) or actin filaments [11].

Microtubules are composed by α- and β-tubulin subunits (50 KDa). These subunits align end to end to form a protofilament that join laterally to form a hollow tube with an outer diameter of 25 nm. Tubulin dimers exhibit GTPase activity that leads to different assembly

pattern. The β-tubulin subunit is exposed at the *"plus" end*, where most of the tubulin dimers are added, opposed to the *"minus" end* that grows more slowly at tubulin physiological concentrations. MTs are assembled differently in dendrites and in the axon. Dendritic MTs are, typically, shorter and often exhibit mixed polarity, with only about 50% of the MTs oriented with the plus end distal facing the tip. On the other hand, axonal MTs (approximately 100 μm long) are uniformly polarized, with all plus ends distal to the cell body. In addition, axonal MTs contain stable segments that, probably, serve to nucleate or organize MTs in axons, particularly during regeneration [11, 12]. The assembly and disassembly of MTs is regulated by microtubule associated proteins (MAPs), categorized in: high-molecular-weight MAPs; tau proteins; MAPs of intermediate molecular weight; and molecular motors (kinesin and dynein). MTs have many functions: they act as a substrate for the transport of membrane-bound organelles (through kinesin and dynein), provide a scaffold for maintaining neurites after extension, and help to maintain the definition and integrity of intracellular compartments during development [11].

Neurofilaments are intermediate filaments (IFs) specific for neurons. All type IV IFs are neuron-specific and form 8- to 10-nm rope-like filaments, several micrometers long, with side arms that project from the surface. These neuron-specific IFs provide mechanical strength and a stable cytoskeletal framework, help to regulate cellular and axonal volumes and are a primary determinant of axonal caliber in large fibers. Finally, NFs exhibit an unusual degree of metabolic stability, which makes them well suited for a role in stabilizing and maintaining neuronal morphology. At least three other IFs occur in selected neurons or neuronal precursors, most prominently expressed during development, and then downregulated in adult: α-internexin (found in CNS and PNS); peripherin (preferentially in PNS) and nestin (in multipotent neuroectodermal precursors) [11].

Microfilaments (MFs) are formed from actin. Actin is a 43 KDa globular protein that exists in its monomeric form (G-actin) and polymerizes into actin filaments (F-actin) to form the actin cytoskeleton. Polymerization of monomeric actin is driven by its ATPase activity, since the hydrolysis of ATP into ADP promotes the incorporation of G-actin into a polymerizing filament. Actin filaments have a diameter of 7 nm and consist of a two-stranded helix of actin monomers. Like microtubules, microfilaments are also polarized structures that exhibit different polymerization dynamics at its ends. The *barbed end* is the fast-growing end of the filament, while the *pointed end* is the slow growing end of the filament. The transition between G and F actin is tightly regulated in cells by a large number of G- and F-Actin-Binding Proteins (ABPs) so that actin filaments represent only approximately 50% of cellular actin. These actin binding proteins also

determine the organization of actin filaments in cells that fluctuate between linear bundles, interconnected networks or contractile structures. For that, ABPs carry out a wide range of functions including actin filament nucleation, elongation, severing, capping, cross-linking and actin monomer sequestration (see figure 2). Generally, ABPs are modular polypeptides that undergo conformational changes in response to signaling cues and transmit these signals to downstream cytoskeletal partners and membranes [10, 11, 13, 14].
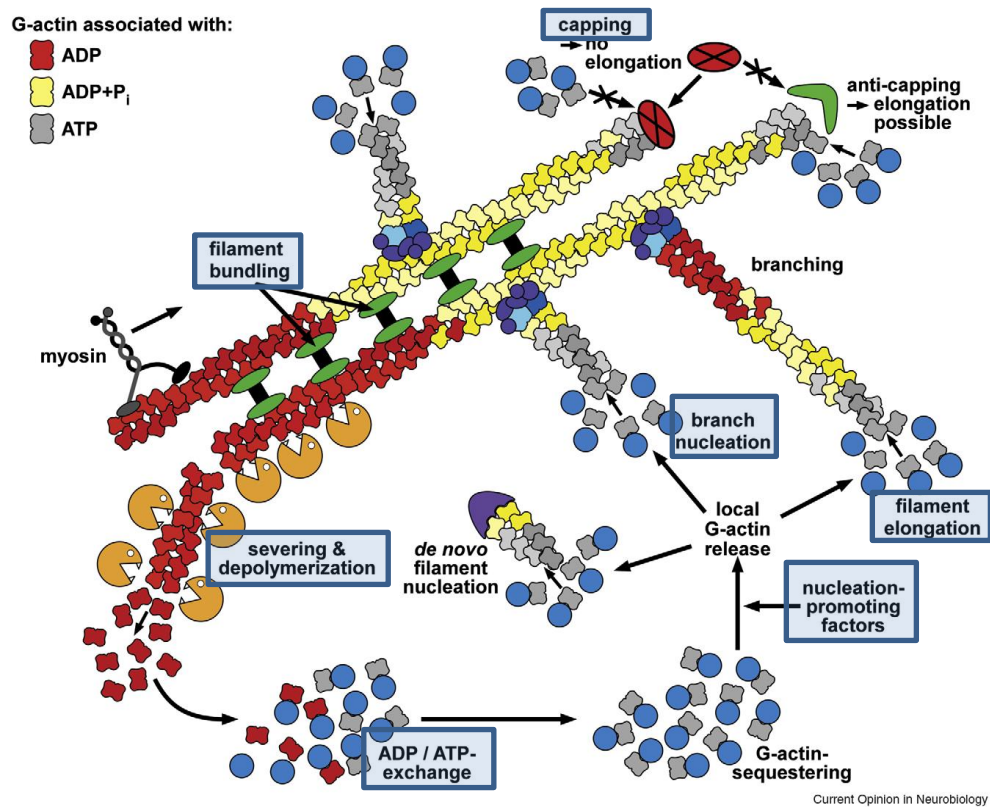
Figure 2 - Actin binding proteins and their functions. ADP/ATP exchanger: <u>profilin</u> – increases the size of actin filaments by binding to actin monomers and enhancing the exchange of ADP to ATP. **Nucleation-promoting factors** modulate actin filament initiation by bringing together actin monomers and pre-existing actin filaments: <u>WASP-family proteins</u>. **Branch nucleation:** <u>Arp2/3 complex</u> – binds both G-actin monomers and the side of actin filaments to nucleate new filaments or branches. **Filament bundling/actin cross-linking** influence the packing and organization of actin filaments into secondary structures: <u>α-actinin</u> – bundles actin filaments; <u>calponin and CaMKIIβ</u> – bundle and stabilize actin filaments; <u>spectrin</u> – cross-links MFs in membrane cytoskeleton via ankyrin; <u>fimbrin</u> – bundles and cross-links MFs. **Capping and severing proteins** promote disassembly of actin filaments: <u>ADF/cofilin</u> – depolymerizes actin through pointed-end sequestering and severing. **Actin filament assembly/filament elongation** can be modulated by events such as controlled nucleotide hydrolysis (e.g. ATP on actin) and reversible modifications (e.g. phosphorylation) on components that control actin assembly. Myosin is an actin-based motor protein that mediates transport and actin contractility [3, 11, 14, 15]. Adapted from [15].

Actin MFs are found throughout neurons, but they are enriched in cortical regions near the plasma membrane and are particularly concentrated in presynaptic terminals, dendritic spines

and growth cones. Most neuronal MFs are less than 1 μm in length and are the main components of the membrane cytoskeleton. The neuronal membrane cytoskeleton plays a role in maintaining the distribution of plasma membrane proteins, establishing cell morphologies and segregating axonal and dendritic proteins into their respective compartments. MFs and the membrane cytoskeleton also mediate the interactions between neurons and the extracellular surroundings, including extracellular matrix components and neighboring cells through the myosin-family molecular motors. In neurons and glia, cell adhesion sites, such as tight junctions and focal adhesion plaques, interact with the MF cytoskeleton either directly or indirectly [10, 11].

1.2. Neuronal growth

Growth control is crucial for neural function as it regulates the number of nerve cells, and the amount and quality of neuronal communication. Neural growth also occurs in adult neuronal networks and it is critical to allow its dynamic adaptation to external environment and to respond to injury. Thus, neural growth can be categorized into three distinct processes: *developmental growth*, in which the construction of the nervous system is included; *plasticity*, the structure remodeling that takes place in the adulthood; and *regeneration/repair*, the response to injury through compensatory modifications or through migration of neural stem cells present in some areas of the brain and differentiation into new nerve cells to replace damaged nerve cells [7]. In adult mammals, neuronal growth is limited to certain CNS sites: adult hippocampus, olfactory bulb, ventricular epithelium and subventricular zone [16].

Neuronal growth is possible through regulation of the structural extension or retraction of neuronal processes (neurites). More specifically, there is an active extension and retraction of the *growth cone* represented in figure 3, which was described by Ramon y Cajal (1890) as a conical expansion at the tips of developing axons and dendrites with finger-like projections (filopodia). Filopodia and lamellipodia, flat membrane veils, consist of two cellular structures fundamental for growth cone motility. These structures can sense the extracellular environment and drive cell motility and migration. Lamellipodia control cell attachment to the substrate, whereas filopodia control the initiation and directionality of growth [10, 14].
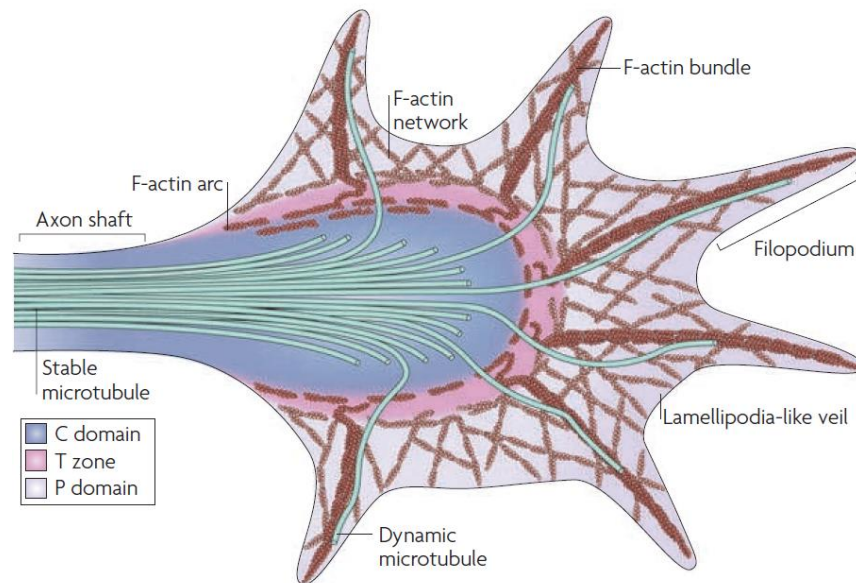
Figure 3 - The structure of the growth cone. The **peripheral (P) domain** contains long, bundled actin filaments (F-actin bundles), which form the filopodia, as well as mesh-like branched F-actin networks, which give structure to lamellipodia-like veils. Additionally, along with F-actin bundles, individual dynamic 'pioneer' microtubules (MTs) explore this region. The **central (C) domain** encloses stable, bundled MTs that enter the growth cone from the axon shaft, in addition to numerous organelles, vesicles and central actin bundles. Finally, the **transition (T) zone** sits at the interface between the P and C domains, where actomyosin contractile structures (termed actin arcs) lie perpendicular to F-actin bundles and form a hemicircumferential ring [17].

The process of neuritogenesis is highly regulated by an intrinsic program activated during early stages of neuronal differentiation and gives rise to the polarized structure characteristic of neurons [5, 10]. Dotti and colleagues observed that the establishment of polarity follows five characteristic stages, when dissociated hippocampal neurons are placed into tissue cultures (see table 2) [6, 8].

Table 2 – Differentiation stages of hippocampal neurons described by Dotti and colleagues. *Adapted from [8]*

Stage 1 0 div	Stage 2 1-2 div	Stage 3 2-4 div	Stage 4 4-15 div	Stage 5 15-25 div

Immediately after attachment, embryonic hippocampal neurons in culture remain as round cells, with a large nucleus, little cytoplasm and a surrounding thin lamellipodia [14]. Lately,

at stage 1, protrusion of lamellipodia and filopodia begins. At the core of filopodia bundles of polarized F-actin extend to the edge of the central domain of the growth cone [18]. This protrusion step generates new intracellular space for cytoplasm, including microtubules and organelles, to move into newly protruded structures. This movement is called "engorgement" [17]. At stage 2, multiple neurites continue to extend, until break of symmetry - specification of an axon – occurs, defining the stage 3. Then, at stage 4, the axon elongates and there is also dendrite outgrowth and branching. Finally, at stage 5 "consolidation" occurs when protrusion is stopped and spines are formed [8, 10].

Growth characteristics of early neurites, including number, morphological characteristics, orientation and speed will be determined by cell and environment specific mechanisms. Cell mechanisms involve the action of adhesion components, membrane turnover and changes in cytoskeletal dynamics [14].

1.2.1. Alterations in cytoskeleton dynamics

Actin (microfilaments) and microtubules are the cytoskeletal structures that form the basis of neurite growth and remodeling. Actin components drive exploratory activity, while microtubules stabilize newly formed processes [6, 15]. The major changes consist of rapid rearrangements of actin filaments in filopodia and lamellipodia of growth cones and net polymerization of microtubules in the neurite shaft. Alterations in actin dynamics are differentially controlled in filopodia and lamellipodia. Filopodia, which function as sensors and extend rapidly, have actin bundles with the growing end towards the tip. Lamellipodia, on the other hand, are filled with an actin meshwork, which is necessary for adhesion and tension for growth cone movement and neurite extension [5, 14]. The remodeling of actin-based cytoskeleton is also an important regulatory step in axon formation. Axon identity is determined in stage 2 of non-polarized hippocampal neurons, by actin-depolymerization in a single neurite that accumulates proteins typical of axons, such as tau, MAP1B and GAP43, a protein involved in actin motility [8, 10]. A model proposed by Andersen and colleagues (2000) describes that a positive feedback loop, once triggered reinforces growth in one neurite to become the axon, while internal inhibitory cues prevent the growth of the remaining neurites [15]. A recent study also suggests that waves, growth cone-like structures that propagate down the length of neurites, occur more frequently in the future axon during initial neuronal polarization. These waves can induce *de novo* neurite branching, increasing actin dynamics [19].

Throughout the remodeling of actin-cytoskeleton, actin monomers are assembled onto the barbed ends of F-actin near the plasma membrane of the growth cone (see figure 4). Polymerization of actin filaments is the major determinant of the extension rate of protrusive structures. However, actin filaments are transient structures and undergo turnover by depolymerization and loss of subunits or by retrograde flow. Depolymerization is regulated by the expression of ADF/cofilin and gelsolin at the boundary of the peripheral and central domain. Retrograde flow acts both in lamellipodia and filopodia and transports actin filaments by a myosin-motor driven process from the periphery of the growth cone to its central domain. This retraction system is prevented by the attachment of F-actin to the adhesion sites on the growth membrane, which enables myosin motors to exert the traction force for forward protrusive activity [10, 18]. The interaction of actin filaments with microtubules connects the functions of microtubules - structural support and organelle transport - to the dynamic cortical actin and to membrane receptors that regulate the motility of a developing neuron. The increased expression of MAPs may stabilize microtubules, enhancing their resistance to the myosin-based forces pulling actin back from the leading margin [5, 10].
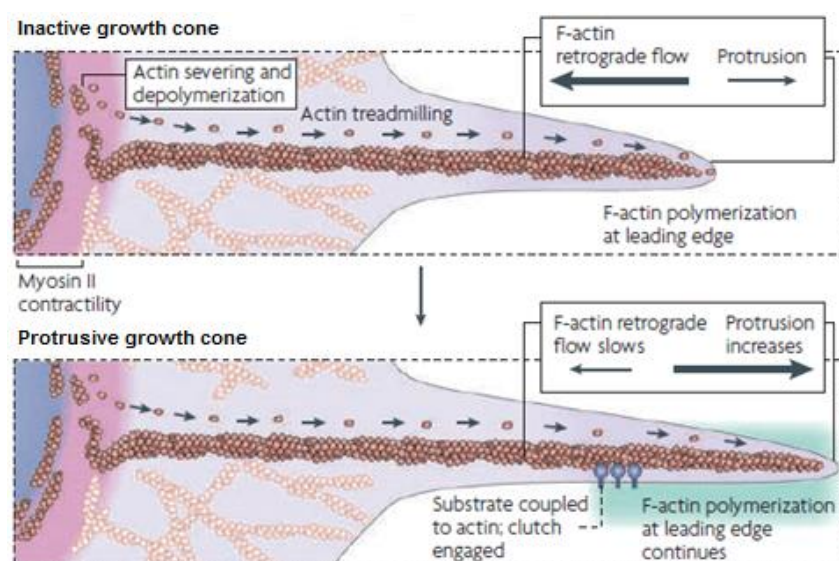
Figure 4 - Actin dynamics at the growth cone: Inactive growth cone: both F-actin treadmilling (in which F-actin is polymerized at the leading edge and severed at the transition (T) zone, with the subunits recycled back to the leading edge) and F-actin retrograde flow (the continuous movement of F-actin from the leading edge towards the center of the growth cone) keep the growth cone inactive. Thus, when retrograde flow and polymerization forces are balanced, no protrusion occurs. **Protrusive growth cone:** when filopodia encounters an adhesive substrate, growth cone receptors bind to the substrate, anchoring F-actin and attenuating F-actin retrograde flow. Further F-actin polymerization pushes the membrane forward, which results in growth cone protrusion. Adapted from [17].

1.2.2. Regulation of neuritogenesis

The formation of specific connections in the developing nervous system depends on the correct pathfinding by growing axons to reach their target cells. Neuritogenesis is influenced by diffusible molecules agents, such as Wnt, netrin and growth factors, and by the biochemistry and geometry of the ECM [20]. These cues generate local differences in the regulation of actin dynamics that can produce growth cone turning if there are variations strong or persistent enough to produce actin based motility. For that, guidance cues must be detected and then the appropriate signaling pathway must be activated [17].

1.2.2.1 The influence of the Extracellular Matrix

The Extracellular Matrix (ECM) is a complex molecular network mainly composed of glycoproteins and proteoglycans from different families, such as laminins, tenascins, fibronectin, thrombospondins, and chondroitin sulfate proteoglycan (CSPGs) or heparan sulfate proteoglycans (HSPGs). Lamellipodia is the first structure to interact with the ECM forming small and highly dynamic complexes called the nascent adhesions characterized by the presence of specific proteins such as Talin, which contains F-actin and integrin binding domains, α-actinin and myosin-II. This complex can dissemble or mature by recruiting a new subset of proteins to become a focal complex and then a *focal adhesion* (see figure 5). Many of these proteins are mechanosensors and thus are recruited by the tension generated by the actomyosin contraction [21-23].

The communication between cell and the ECM is made through adhesion receptors that can be divided into: integrins, which mediate cell adhesion to the ECM; cadherins and IgCAMs that mediate principally cell-cell adhesion but can also recognize and bind some ECM molecules [23]. The integrin family of membrane receptors is composed of numerous α- and β- subunits that dimerize on the cell membrane and link it to the extracellular matrix and to the actin cytoskeleton. Evidence suggests that the functionality of these integrins requires an activation step through a conformational change correlated with a high binding affinity to the ligand and clustering into cell junctions. Once integrins are activated a variety of intracellular responses are initiated, including the phosphorylation dependent recruitment of signaling proteins that regulate filopodia protrusion and cell proliferation (see figure 5). Several studies addressed the role of calcium in this mechanism, revealing that the exploring filopodia in the growth cones generates localized elevations of intracellular calcium through the activation of integrin receptors [14, 23, 24].
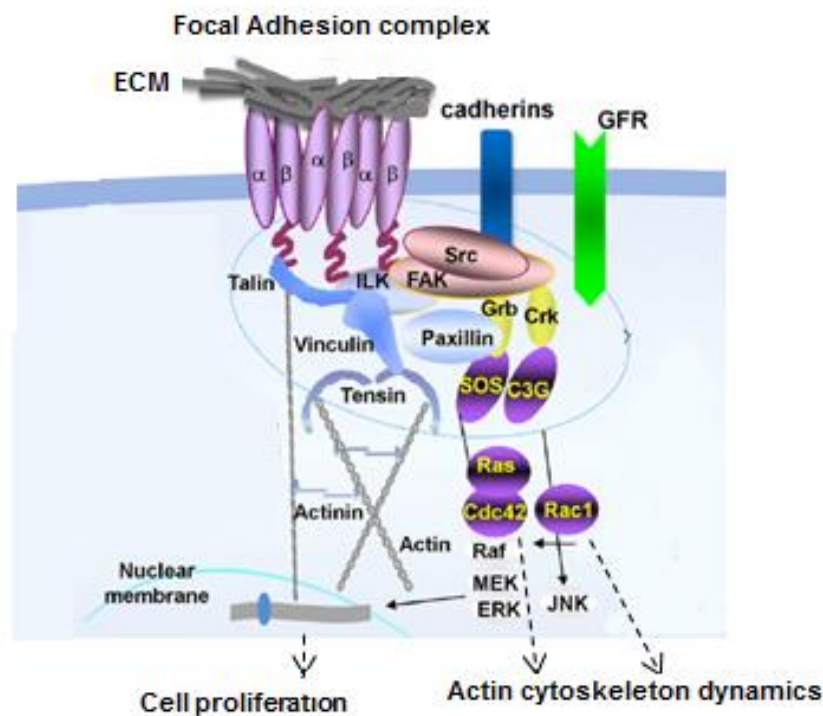
Figure 5 - Focal adhesion schematic diagram. Focal adhesion (FA) is assembled by integrin clustering and induces recruitment of cytoskeleton binding proteins, such as talin, vinculin, actin, tubulin, actinin, paxillin and tensin, and non-receptor tyrosin kinases such as adhesion kinase (FAK) and Src to the focal contact. Other proteins recruited to the FA control important cellular events such as cell proliferation and cytoskeleton dynamics alterations. Adapted from [25, 26]

Particular sets of ECM proteins have shown to play a role in the regulation of the number, direction, extension, and retraction of neurites [27]. While many of them stimulate neuritic outgrowth, others have restrictive effects. Laminin, fibronectin and several collagens promote neuritic outgrowth. This stimulating effect might be induced by adhesion, via integrins, that reduces membrane tension in specific sites where filopodia or lamellipodia will extend. Thus, regulation of integrin activity is one of the important mechanisms that controls neurite outgrowth [14, 23].

1.2.2.2 Diffusible chemotropic cues

In addition to the ECM, diffusible chemotropic cues provide further steering instructions to the growth cone. Until recently, it was assumed that the intrinsic properties of these molecules would determine the growth cone response of attraction or repulsion; however, it is now clear that specific growth cone receptors are responsible for the activation of these opposite intracellular responses [17]. Table 3 summarizes the effects of different signals that regulate growth cone progress.

Table 3 – Effects of diffusible chemotropic molecules on growth cone dynamics.

Signal	Attractive response	Repulsive response	Ref.
Netrin	Coordinates axon initiation *in vivo*; Causes localized activity of PI3K, development of directed actin-based protrusions and axon specification.	Can also induce repulsive effects.	[8, 10]
Wnt	Regulates axon specification and neuronal polarity.		[8, 15]
Neurotrophins *NGF – nerve growth factor* *BDNF – brain derived neurotrophic factor* *NT-3 and NT-4 neurotrophin-3 and 4*	Increase of total dendritic length; Increase of the number of branch points and/or number of primary dendrites; BDNF - plays a role in directing axon specification; NGF – dependent outgrowth: mediated by integrins; Neuronal activity can significantly enhance axonal growth stimulated by trophic factors.		[6] [8] [23] [28]
Sema3A	<u>In dendrites</u>: High expression of enzyme soluble guanylate cyclase (sGC), that regulates cGMP production; Sema3A + high cGMP levels: actin polymerization and dendritic growth.	<u>In axons</u> Sema3A + low cGMP levels: activation of GTPase RhoA → depresses actin dynamics and activates myosin II contractility.	[6]
Myelin-derived growth inhibitory proteins		Inhibit axonal extension; Causes neurite retraction; Lead to growth cone collapse; Expressed after injury in the PNS, but also present during neural embryogenesis; The effects of these proteins are mediated by the activation of RhoA and inactivation of Rac.	[10]

1.2.2.3 Signaling pathways activated during neuritogenesis

Several signaling pathways have been identified as central players in the transduction of extracellular signals to downstream effectors. Rho, integrin and calcium signaling will be here explained in more detail, while other signaling pathways are summarized in table 4.

Ras-and Rho-Family of small GTPases: Rho GTPases are proteins of the Ras superfamily that are active when bound to GTP and inactive when GTP is hydrolyzed to GDP. These proteins are regulated by three protein families: *GEFs* that catalyzes GDP release and induce GTP binding (activators), *GAPs*, which promote GTP hydrolysis (inhibitors), and *GDIs* that inhibit GDP dissociation (inhibitors). Rho GTPases interact with many downstream effectors that are involved

in most intracellular processes requiring alterations in actin dynamics such as cell migration and cytokinesis and alterations in both actin and microtubule dynamics, such as cell differentiation. So far, ten members of Rho GTPases have been identified, however only three of them are well-studied: RhoA, Rac1 and Cdc42 [6, 8, 10, 13].

RhoA is normally inactive; however its local activation is suggested to lead to a dramatic decrease in dendritic growth and to induce retraction of existing branches due to stress fiber and focal adhesions formation. *Stress fibers* consist of bundles of microfilaments and other proteins that are commonly found on migrating cells and can be anchored to a focal adhesion. These effects appear to be mediated by Rho-associated Kinase (ROCK), which has been shown to have effects in the activation of actomyosin-based contractility and suppress microtubule assembly in neuroblastoma cells. ROCK is a serine-threonine kinase that interacts with GTP-bound active RhoA and induces acto-myosin contraction through inactivation of myosin light chain (MLC). Furthermore, ROCK also inactivates ADF/cofilin through LIMK to induce actin filament stabilization which is important for myosin contraction [10, 14].

Rac1 and, to a lesser extent Cdc42, induces a rapid restructure of dendrites with an increase in dendrite branch additions and retractions. These effects might be mediated by the same effector, probably PAK1 that is activated by Rac1 and Cdc42 and has been shown to induce neurite formation in PC12 cells. PAK enhances actin filament elongation and acto-myosin contraction. Proteins that interact with Cdc42 and Rac contain a short stretch of ~18 amino acids referred as the Cdc42/Rac Interactive Binding (CRIB) motif, which has been identified in a number of potential Rho-family effector proteins, such as WASP, formins and IRSp53 [8, 10, 13].

Integrin signaling: FAK is a non-receptor tyrosine kinase that is activated by integrin engagement. This protein is also a large adaptor protein with binding sites for many proteins involved in cell signaling and motility including several growth factor receptors, integrins, PI3K, Src, Rho GTPases regulators and cytoskeletal proteins. *In vitro* (PC12 and SH-SY5Y) and *in vivo* studies have shown that FAK activation promotes neuritic outgrowth and inhibition of axonal branching [23].

Calcium and electrical activity – calcium is established as a key mediator of the regulation of neurite outgrowth [5]. Changes in the intracellular concentration of calcium regulate growth cone responses to neurotransmitters, electrical activity and neurotrophic factors by modulation of the state of polymerization of actin filaments and microtubules [5, 18]. Electrical activity leads to an increase in neurite initiation, faster elongation and navigation towards the cathode of the applied field. Its effects can be attributed to an electrophoretic redistribution of surface receptors

and to the influx of Ca^{2+} that can be global or localized. It has been observed that the global increase of intracellular calcium levels reduces the elongation rates of axons and dendrites, whereas local increases in $[Ca^{2+}]$ have a directing effect. During the establishment of polarization, several Ca^{2+} dependent effector proteins, which play different roles in regulating the growth cone, are activated. CaMKII, for example, is highly enriched in neurons and phosphorylates many substrates that are involved in neurite growth. Gelsolin, on the other hand, is a severing protein that localizes to the growth cone and initiates filopodia retraction. Many of these proteins are involved in regulation of actin dynamics, indicating that calcium can trigger the polymerization and rearrangement of F-actin to extend filopodia [18].

Table 4 – Important signaling pathways in neuritogenesis. Adapted from [8], [10], [29].

Pathway	Function
LKB1, SAD-A/B and MARKs	LKB1 is activated by BDNF; LKB1 phosphorylates: - SAD-A/B kinases: direct pre-synaptic vesicular trafficking in the neurite becoming the axon; - MARK1-4: phosphorylates microtubule associated proteins such as Tau.
PI3K and PTEN	PI3K: - Regulator of neuronal migration and polarization: PIP3 accumulates selectively within a single neurite following application of laminin specifically to a single neurite of stage 2 hippocampal neurons; PTEN: - dephosphorylates PIP3 to form PIP2, decreasing the accumulation of PIP3 and thus leading to a loss of axon formation
GSK3	Critical regulator of neuronal polarity (its inhibition leads to the formation of multiple axons)
RAF/MEK/ERK	ERK and MAPK: regulate many transcription factors required for growth responses, and also the axon cytoskeleton by phosphorylation of several microtubule associated proteins.
JNK	Phosphorylates various cytoskeletal proteins that regulate axon extension, such as MAP1B and MAP12.
Notch	Type I cell surface protein: receptor for a diversity of signals that can influence dendritic morphology - positive role in dendrite branching and a negative role in dendrite and total neurite length.

1.3. CNS and PNS injury

Spinal cord injuries and neurodegeneration are major causes of CNS injury and have been studied for many years in order to understand the mechanisms that lead to failure of neuritic re-growth and how the intrinsic growth potential can be enhanced. In neurodegenerative diseases there is an accumulation of insoluble filamentous aggregates which lead to early axonal

dysfunction and consequently causes irreversible neuronal degeneration. Spinal cord injuries and brain trauma, on the other hand, damage neurons and trigger an injury response that prevents the reestablishment of its normal function [30].

1.3.1. Neuronal and non-neuronal injury responses

Neuronal cell body response to injury differs from axonal response. In the cell body Nissl substance disperses, the nucleus is displaced to the cell's periphery and swelling of the cell body (hypertrophy) and loss or retraction of synaptic terminals, occurs. Even though these responses are equal between CNS and PNS, long-term cell body responses vary between regeneration competent and incompetent neurons. In regeneration-competent neurons, such as spinal motor neurons, the cell bodies remain hypertrophic and show signs of increased metabolism and protein synthesis. On the other hand, regeneration-incompetent neurons appear atrophic, display reduced cell volume and dendritic arborization. The axonal compartment also undergoes through specific alterations including self-destruction by Wallerian[1] degeneration and sealing of the axonal membrane which takes several minutes to an hour [31]. In regeneration-competent neurons, the cut axonal end transforms into a growth cone-like structure to integrate extracellular signals and orchestrate the use of materials for axon regrowth (see figure 6). This final step is critical for axon regeneration and depends on the neuronal type. While PNS neurons are able to initiate regenerative growth, in CNS neurons, abortive sprouts is more likely to occur [28].

After injury, the cell body has to be informed about the neuritic transection; this may happen by: cell damage itself, changes in the neuritic milieu produced by inflammation or scarring and/or alterations between neuron's partners. Then, parallel alerting pathways are activated. Changes of ionic concentrations and electrical activity in injured neurons are one of the earliest injury-related signals. A local increase of calcium concentration, for example, is necessary to induce the formation of a growth cone and to promote its assembly [5, 18]. Furthermore, the cell body might also be informed of the damage by the interruption of the flow of gene expression inhibition produced by the axonal environment and/or by production of positive signaling molecules like cytokines and neurotrophic factors [7, 10]. Several studies in dorsal root ganglia have shown that a first injury at the peripheral branch can increase the regenerative response to a second lesion occurring at either a peripheral or central branch. A peripheral injury might trigger

---

[1] Wallerian degeneration is the set of molecular and cellular events by which degenerating axons and myelin are cleared after injury.

a recapitulation of the developmental patterns of expression of growth associated proteins, transcription factors and translational regulators [28].

Non-neuronal components of the nervous system, including neuroglial cells show varied responses after axotomy in PNS and in CNS. In the PNS, there is a quick clearance of the axon and myelin debris. On the contrary, this process is more slowly in the CNS and specific glial responses are initiated [28]. There is the formation of a glial scar, composed of astrocytes, ECM proteins, myelin and oligodendrocytes. TGFβ is one of the molecular cues that contributes to the initiation of reactive gliosis immediately after injury [32]. The glial scar is an evolving structure characterized by the presence of different cell types that reach the injury site at different times. Macrophages from the bloodstream and microglia from the surrounding tissue arrive within hours of injury. Then, 3-5 days after, oligodendrocyte precursors are recruited from the surrounding tissue. Finally, astrocytes divide and migrate to the injury site, and eventually fill in the vacant space. Besides acting as a simple mechanical barrier, the biochemical changes produced by tissue damage at the injury site affect local outgrowth of nerve process [4, 33].

1.3.2. Intrinsic growth and regenerative potential

The mechanisms that contribute for intrinsic growth potential after neural injury can be divided into *constitutive plastic properties* that reflect the basal level of expression of growth molecules in an intact neuron and the *regenerative potential* that reproduces the ability for reactivating their synthesis in response to injury [7]. Until recently, it was assumed that axonal regeneration in CNS was impossible. However, many studies have shown that, when provided an appropriate environment, axons of the adult mammalian CNS can regenerate. These new data indicated that CNS neurons have some intrinsic potential for growth [31]. In order to restart neuritogenesis after neural injury, neurons have to undergo structural remodeling and *de novo* activate specific genes. Local cytoskeletal rearrangement occurs in the axon terminal aiming to growth cone reformation and sprouting. Cell body response is required for the synthesis of raw materials for axon growth, namely transport and assembly of axonal components along the axonal shaft and at the terminal. As mentioned before, the axon may also be partially autonomous in protein synthesis, what in addition to axonal transport can overcome the long distance between the soma and the axon terminal (in various neurons). So far, mRNAs for cytoskeleton elements (microtubules, microfilaments and intermediate filament proteins), signal transduction mediators, metabolic and anti-oxidant enzymes, heat-shock proteins and molecules related to neurodegenerative disorders have been identified in the axon. Even though GAP43 and

α-tubulin, proteins associated with axon regeneration, have not been identified in the axon, mRNAs for β-actin, cofilin and tropomyosin have been detected in regenerating axons. These results suggest that even though some *de novo* transcription might be required for a full regenerative response, local protein synthesis may contribute to increase actin dynamics and growth cone motility. In fact, local protein synthesis is under fine regulation and responds to guidance cues, neurotrophins and axotomy in order to induce an immediate response in the neurite and modify its sensitivity to ensuring signals [7, 8, 10, 28].

Regenerative potential is dependent on the neuron age, its particular phenotype and the specific injury conditions. Thus, a full regenerative response is more likely to happen in young PNS neurons, with injury close to the cell body. This happens because neurons in early developmental stages possess robust axon growth and regenerative ability. In PNS neurons, the inhibitory cues are less prominent. Finally, the probability of a new axon forming following injury to initial axon was related to the distance from the cell body at which the axon injury occurred, with probability decreasing with increasing distance from the cell body [5]. Conversely, results from optic nerve regeneration suggest that the critical factor is the length of the remaining myelinated axon segment along the axon [7].

1.3.3. Determinants of axon regeneration failure

A possible reason for failure of regeneration in CNS neurons might be their inability to translate signals that are activated after injury [28]. In addition, a gradient of inhibitory extracellular matrix molecules also produces long distance regeneration failure. These factors include poor clearance of damage tissue caused by slow Wallerian degeneration, scarring caused by astrocytes and the presence of myelin-associated axonal growth inhibitors [34, 35]. Besides the existence of a mechanical barrier due to the formation of the glial scar, the biochemical changes produced by tissue damage at the injury site affect local outgrowth of the nerve process. Proteins released from degenerating myelin and by glial scar formation contain repulsive molecules, such as sema3A, ephrin-A2 and chondroitin sulfate proteoglycans. These proteins inhibit growth cone adhesion and activate RhoA signaling to limit actin polymerization, trigger myosin II contractility and inhibit growth cone advance [4, 7].

Some of the molecules released after neural injury are pro-inflammatory and can lead to upregulation of inhibitory molecules; however, they also provide neuroprotective benefits during the healing process. Further, macrophages can secrete factors that are growth promoting, such as NGF and NT-3 also enhancing the regenerative response [4].

Consequently, the final outcome of the repair process will be determined by the reciprocal interactions between intrinsic neuronal growth properties, molecular cues in the CNS and the specific nature of incoming external stimuli as depicted in figure 6 [7].
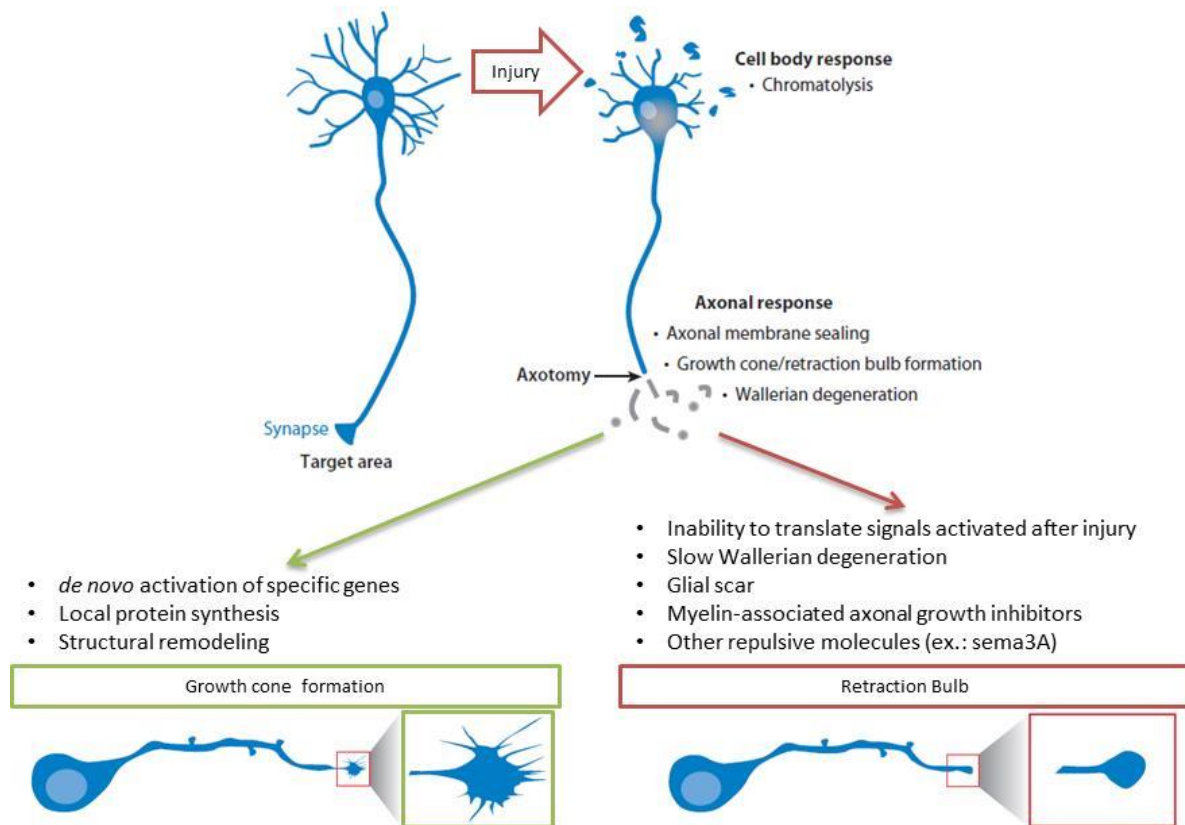
Figure 6 – Neuronal injury responses and final outcome. The cut axon end might assemble into a new growth cone, or a retraction bulb will be formed if the intracellular and extracellular cues inhibit the transformation. Adapted from [28]

1.4. Tissue engineering based therapies

The current treatments of CNS injury aim to minimize secondary injury and implement physical therapy designed to help patient function with limited mobility [32, 34]. Several approaches have been put forward for axonal regeneration. Antibodies and enzymes to block growth inhibitors and to promote axon growth motility could stimulate actin dynamics and promote axonal regeneration. However, adult CNS neuron's growth potential is greatly decreased when axons reach their targets. Thus, strategies for regeneration of CNS axons goals should be to prevent the inhibitory molecules and to increase growth-promoting molecules of the CNS environment. In addition, these strategies should change gene expression in injured neurons to

re-express the cytoskeletal components and signaling activities that characterize developing neurons [10].

Artificial tissue scaffolds are designed to provide mechanical support for axonal regrowth and potentially to serve as a local delivery system for growth factors and/or as a carrier for living cells that might facilitate repair [34]. These tissue engineering based therapies hold a great promise for CNS and PNS regeneration. In CNS, tissue regeneration aims to repair functional tissue and restore sensory and motor function. In PNS, although "natural" regeneration is possible, the healing process is slow, about 0, 5 - 1 mm/day. Thus, tissue engineering strategies might help to speed up regeneration [32].

The design of these scaffolds for neuronal regeneration should meet minimal safety and functionality criteria: biocompatibility with the host tissue and production of an extremely low inflammatory, immunogenic and cytotoxic response; adjustable rate of degradation and production of nontoxic degradation products; match its mechanical properties with the properties of the lesion site and render permeability to the entry of nutrients but still act as the necessary barrier to prevent the infiltration of unwanted tissues; provide a three-dimensional support since cells are located in a 3D microenvironment surrounded by other cells and by the ECM; finally, it should promote cell adhesion and axonal regrowth and be able to reduce astrocytic reaction and fibroblastic gliosis [34, 36-39].

One of the most important characteristics of the design of tissue scaffolds for neuronal regeneration is to simulate the structural and physical properties of soft brain tissue. Thus, to replicate the essential intracellular reactions and promote native intracellular responses, the ECM must be mimicked in a scaffold material that is able to interact with cells in three dimensions and facilitate this communication. In native tissues, the structural ECM proteins (50- to 500-nm-diameter fibers) are one to two orders of magnitude smaller than the cell itself; this allows the cell to be in direct contact with many ECM fibers, thereby defining its 3D orientation [36]. This property may be a crucial factor in determining the success or failure of a scaffold. Topographical characteristics of the scaffolds will determine how biological molecules are adsorbed onto the substrate, particularly its orientation, and it will regulate important characteristics of cells in contact with the substrate such as cell morphology, rates of movement and cell activation [40]. Therefore, tissue engineering research has focused on nanotechnology for the development of scaffolds for neuronal regeneration.

1.4.1. Nanomaterials and their potential for neuronal regeneration

Nanotechnology emerged in 1959, when the physicist Richard Feyman recognized the potential of manipulating individual atoms and molecules at the nanometer scale (see figure 7). This pioneering technology allowed the development and use of nanometer-scale materials that display unique functional properties, such as nanotubes, nanofibers and nanoparticles [41-46].
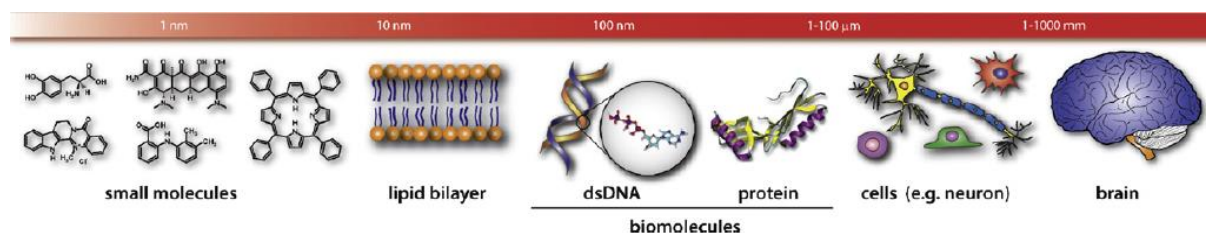
Figure 7 - The nanometer scale. Left to right: Small molecules, such as dopamine, minocycline, mefenamic acid, DHED, and heme, are approximately 1 nm or smaller. The lipid bilayer is a few nanometers thick. A biomolecule such as a (22 bp) microRNA and a protein is only a few nanometers in size. A single cell or neuron is tens or hundreds of microns in size. Human brain is tens of centimeters in size. *Adapted from* [46].

Nanomaterials have become promising candidates for a variety of tissue engineering applications. These nano-scale materials display advantageous properties for neural applications. There is an increased surface to volume ratio and surface area that allows a greater degree of surface interactions and consequently, increased surface energy. Thus, nano-features promote the adhesion of surrounding cells to scaffolds and the infiltration of neuronal and glial processes upon injury response [32, 43, 47, 48]. In addition, mechanically robust scaffolds with high porosity and interconnected pores can be designed so that there is more structural space for cell accommodation and nutrient and metabolic waste can be exchanged between the scaffold and the environment [49]. Furthermore, nanomaterials are biomimetic and can resemble native tissue, since ECM proteins have dimension on the nanoscale. Nano-features can be arranged to provide topographical guidance cues that have been shown to affect neural cell function. Random topographical features were found to enhance cell adhesion and spreading, while ordered topographical features have been shown to induce the orientation of focal contacts and promote neurite outgrowth [40].

Topographical features and other characteristics of nanomaterials can be defined rendering the fabrication technique used. These techniques can be divided into three groups: conventional methods, textile technologies and solid free form fabrication, described in table 5 [34, 47].

Table 5 – Techniques used for the design of nanomaterials [36, 47].

Group	Techniques	Characteristics
Conventional methods	Solvent-casting Particulate-leaching Gas foaming Phase separation Melt molding Solution casting Freeze-drying	Lack the ability to precisely control the pore size, pore geometry and spatial distribution of pores within the scaffold.
Textile technologies	Electrospinning	Possess the ability to generate nanofibrous structures with controlled fiber diameter and orientation; Simple and cheap method to fabricate nanofibers with diameters similar to certain ECM microstructures; Difficult to control fiber morphology with other parameters such as solution properties, governing variables and ambient parameters.
Solid free-form fabrication	Computer aided fabrication process	Control of the physical properties of a scaffold: pore size, porosity, interconnectivity and mechanical strength. Better cell seeding in scaffolds interior, lower cell oxygen gradients.

Electrospinning represents an attractive technique for the processing of polymeric biomaterials into nanofibers that resembles the size scale of the subcellular level (< 1 μm) [36, 41]. To produce a nanofibrous scaffold using electrospinning the material to be electrospun is first dissolved in a suitable solvent to obtain a viscous solution. This solution is first passed through a spinneret, and a high voltage supply is used to charge the solution. At a critical voltage, typically 10 – 30 kV, the repulsive forces of the charged solution particles result in a jet of suspension erupting from the tip of the spinneret [36, 50].

The morphology, fiber diameter and porosity of electrospun nanofibrous scaffolds can be controlled by varying parameters, such as applied electric field strength; spinneret diameter; distance between the spinneret and the collecting substrate; temperature; feeding rate; humidity; air speed; and properties of the solution or melt, including the type of polymer, polymer molecular weight, surface tension, conductivity, and viscosity, temperature, concentration of the polymer [49]. Fiber alignment can be achieved by varying the collection method. The most common methods consist in collecting the solution on a high speed rotating drum or disk what allows for the fiber to collect along the direction of rotation. A high rotation speed produces increased fiber alignment as compared to lower rotation speed, but may cause fiber discontinuity [51]. Fiber diameter is also an important parameter to consider during the design of nanofibrous scaffolds. It can influence cell adhesion, proliferation, migration and differentiation. [50]. Various

studies show that larger-diameter fiber substrates yield higher cell densities than smaller-diameter fiber [52, 53]. Along with the fabrication technique, different materials from different sources and with different characteristics can be used to design nanomaterials for neural regeneration. They can be natural or synthetic materials. Natural materials possess similar properties to the tissues they are replacing and may contain specific signals for cell adhesion, allowing for cell infiltration. However, they may present some disadvantages such as induction of immunological response or need for some modifications for better degradation and for axon growth due to its weak mechanical properties [34, 36]. Therefore, synthetic materials can overcome these problems as they have a known composition and can be designed to minimize the immune response and facilitate enhanced axon regeneration. Furthermore, they can be bioresorbable, non-toxic, easy to sterilize and low cost [41, 54]. Table 6 describes some neuronal and glial cell response to different nanomaterials.

Table 6 – Main nanomaterials' biological activities.

	Material	Model	Results	Ref.
Natural	Collagen	SK-N-MC Human normal fibroblast hNP-AC	Biocompatibility of scaffolds to the cells Parallel alignment of cells to the orientations of collagens nanofibers	[55, 56]
	Agarose	Ascending spinal cord sensory axons (mouse)	Can guide long tract axons through a spinal cord lesion site	[57]
Synthetic	Polycaprolactone [PCL]	HaCaT (Keratinocyte cells) NG108 -15 cells and Schwann cells (Neuroblastoma-glioma hybrid) Neonatal mouse cerebellum C17.2 stem cells PC12 cells	Support neurite extension; Promote Schwann cell growth and migration Coated with polypyrrole (PPy): electrically conductive surface promotes neural stem cells differentiation [↓nestin, expression of NF-H, MAP2, GFAP, APC]; Blended with PAni: enhanced NGF-induced neurite outgrowth [↑GTP-RhoA, Cdc-42, Rac, ↓caspase 3];	[39, 58-61]
	Poly(L-lactic) acid [PLLA]	Neonatal mouse cerebellum C17.2 stem cells Primary motor neurons Mouse Embryonic stem cells (ESCs)	<u>Random fibers</u>: Randomly oriented cells with spindle and polygonal morphology. <u>Aligned fibers</u>: Cells spread along the long axis of the aligned fibers; Longer neurite length; Accelerate neuritogenesis; Blended with carbon nanotubes: enhanced the expression of mature neural; markers [MAP2 and NSE].	[20, 40, 54, 62-65]
	Poly(lactic acid-co-glycolic acid) [PLGA]	Neural stem cells	Promoted NSC migration and differentiation; Help to establish a neural network with synaptic activity.	[66]
Composite	Gelatin/PCL	Schawnn cells Mesenchymal stem cells	Increased proliferation and cell attachment Encapsulating Retinoic Acid (RA): ↓cell proliferation, ↑Tuj-1 and MAP2	[49, 67]

Various modifications can be made in nanomaterials to enhance their regenerative properties:

Modification of nanomaterials to mimic the ECM: The incorporation of ECM proteins or peptides into biomaterials can influence a variety of cellular process including cell migration, axonal guidance, synaptogenesis, survival, differentiation and myelination. PLLA nanofibers, for example, can be coupled with laminin using different methods: covalent binding using water soluble carbodiimide and N–hydroxysuccimide as coupling reagents, physical adsorption and physical blending of laminin with the PLLA solution before electrospinning [68].

Incorporation of growth factors: The incorporation of growth factors into electrospun scaffolds would be of interest to regulate proliferation and differentiation. Several studies revealed an increase of cell proliferation and differentiation when BDNF was immobilized in the scaffolds [50].

Incorporation of living cells into tissue scaffolds: This strategy can increase regeneration because these cells can produce necessary bioactive molecules, promote axon growth and eventually promote myelination of regrown axons. Schwann cells, olfactory ensheathing cells and embryonic stem cells have been used in experimental SCI therapies and bring forth encouraging results [34].

Electrical stimulation: fibers that incorporate electrical activity may modify cellular activities such as cell migration, cell adhesion, DNA synthesis and protein secretion. Data from *in vivo* and *in vitro* models support the hypothesis that a loss of electrical activity promotes neuronal degeneration and that exogenous electrical activity promotes neural survival [34, 50, 54, 61].

1.4.2. PLLA and its piezoelectric properties

Poly L-lactic acid (PLLA) is classified as a poly (α-hydroxy esters). These polymers are readily made into 3D scaffolds that biodegrade via hydrolysis in CO_2 and H_2O, resulting in their bioresorption in the Krebs metabolic cycle [36]. PLLA, which chemical structure is depicted in figure 8, is one of the most commonly used polymers due to their source and characteristics – synthetic, biodegradability and biocompatibility [50].
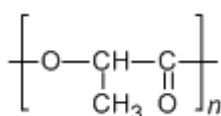

Figure 8- Chemical structure of Poly L-lactic acid (PLLA).

Yang and colleagues published in 2005 the first electrospun aligned PLLA scaffold for neural application. In this paper they demonstrated that neural stem cells differentiated when cultured onto aligned PLLA nanofibrous scaffolds, and thus it could be a potential cell carrier in neural tissue engineering [65]. The potential of PLLA scaffolds for regeneration has also been studied in other tissues including: hepatic [69], vascular [70] and bone tissue [71].

PLLA is a dielectric material, what means that when an electric field is applied on PLLA no current flows within the material because there are no free charged particles within the material to conduct the current. Nevertheless, PLLA is also characterized as degradable piezoelectric material. Piezoelectricity (from the Greek piezo or piezein (πιέζειν) ≈ squeeze or press | electric or electron (ήλεκτρον)) was discovered in 1880 by Jacques and Pierre Curie and consists in the production of electricity in response to mechanical stress. Early in the 1950s, Fukada found piezoelectricity in various kinds of biopolymers [72]. This phenomenon is related to the change of dipole crystal orientation when a force is applied. The dipole structures in a piezoelectric material are organized and no net charge is produced at rest. When a mechanical force is applied, the shifting or rotation of the dipole crystal results in the change of polarization density, hence, causing the transient change of electric charge. Upon the removal of mechanical force, the dipole crystal returns to its original space [50]. This is considered as the direct piezoelectric effect. However, the piezoelectric materials also present a reverse piezoelectric effect, being able to generate mechanical strain in result of an applied electrical field. In the case of polymers, the piezoelectricity is enhanced by the dipolar orientation within the material, either by electrical polarization or mechanical stretching.

This is a key property of PLLA for tissue regeneration application as it induces a transient change in surface charge without requiring additional energy sources or electrodes. This property has already been tested in bone. The piezoelectric polarization in PLLA caused by mechanical tension induces electric current in bone, which stimulates the biological activity of osteocytes and accelerates the growth of bone [72]. Recently, piezoelectric polymers based on a non-degradable synthetic polymer – polyvinylidene fluoride (PVDF) have been studied for wound healing [73] and neural repair applications [74]. The piezoelectric nature of this electrospun scaffold may be induced *in vitro* via deformations of the fibers due to cell attachment and migration [74]. *In vivo* and in view a neuronal regenerative approach, activation of piezoelectric activity might be achieved by the cerebrospinal fluid circulation, by the motion of neighboring anatomical structures of the peripheral nervous system and/or in combination with other therapeutic strategies such as ultrasound [74, 75].

The electrical stimulation provided by a piezoelectric polymer initiates molecular signaling of survival and neurite outgrowth through protein synthesis, post-translational modifications, or alterations in gene expression that provide neuroprotection and promotes axon growth. The expression of neurotrophic factors and the sensitivity to these signals, for example increases upon electrical stimulation. The responsiveness to neurotrophic factors, induced by elevating cAMP creates an increase in the levels of neurotrophic factor receptors on the cell surface and also increases receptor gene expression over a long term. The increase in cAMP might be attributed to the activation of calcium dependent adenylyl cyclases (AC) [16, 76]. Results from electroacupuncture therapeutic technique for spinal cord injury suggest that the pulse electric field causes the depolarization of neurons and glial cells, resulting in the opening of voltage-gated ion channels, leading to rise in the intracellular calcium level and subsequent autocrine release of neurotrophic factors such as NT3 [77].

In conclusion, a PLLA nanofibrous piezoelectric scaffold would be the ideal scaffold for neural regeneration as it combines the ECM-like topography, biodegradability and the possibility to produce electrical charge to enhance neurite outgrowth. To evaluate the effectiveness of this strategy, cell assays (viability, proliferation, adhesion) and protein expression assays must be performed and then, *in vivo* assays should be used to check its security and efficacy.

2. Aims

In the present work, the cellular responses to non-polarized and polarized PLLA samples (films, random and aligned nanofibers) were assessed in order to evaluate their ability to promote neuronal differentiation, in view of their potential regenerative application. Therefore, the main objectives of this dissertation were:

- To assess the ability of neuroblastoma SH-SY5Y immortalized cells to adhere to the various PLLA samples;
- To evaluate the biocompatibility of PLLA samples by assessing their effect on SH-SY5Y cells viability (metabolism, apoptosis);
- To study the effects of PLLA samples on SH-SY5Y cell morphology, and on cytoskeleton dynamics;
- To evaluate the effects of PLLA samples on neuronal-like differentiation and on neuritic outgrowth.

3. Materials and methods

3.1 Cell culture with PLLA samples

SH-SY5Y human neuroblastoma cells are originally derived from the cell line SK-N-SH, established from a bone marrow biopsy of a neuroblastoma patient. The SH-SY5Y cell line (ATCC, Barcelona, Spain; CLR-2266) was maintained at 37ºC in a humidified atmosphere of 5% CO_2, in 10% fetal bovine serum (FBS) minimal essential medium (MEM):F12 (1:1), with 2 mM L-glutamine, 100 U/mL penicillin and 100 mg/mL streptomycin (10 mL Streptomycin/Penicillin/ Amphotericin solution, Gibco). Cells were split at 70 – 80% confluence. Before cell seeding, PLLA films and nanofibers (random and aligned) were cut into squares of 1 cmx1 cm and sterilized by two means. Polymers were sterilized with 70% ethanol for 5 min, and washed with: distilled water (10 min), washed twice with 1x PBS (10 min), and further incubated for 3h with SH-SY5Y culture medium. Alternatively, polymers were sterilized under an UV lamp (30 W, 25 nm), overnight. Cells were then seeded on the polymers in 24-well and 12-well plates at the indicated cell densities, upon scoring their number with the Trypan blue assay.

3.2 Trypan Blue assay for initial cell plating

In order to plate a defined number of living cells, a dye exclusion assay was used, in which living cells with an intact cytoplasmic membrane exclude the reagent, while dead cells stain blue due to dye incorporation through permeabilized damaged cytoplasmic membranes. To an aliquot (90 µL) of cells suspension, 10 µL of 0,4% Trypan Blue were added and incubated for 1 minute at room temperature. The unstained (viable) cells were counted in a haemocytometer (0,1 µl), and cell concentration calculated for further cell plating.

3.3 Laminin-coating

PLLA samples and control wells were coated with laminin according to the *physical adsorption method.* Laminins are heterotrimeric glycoproteins with binding regions for collagen, integrins, cellular domains and proteoglycans [68]. PLLA films and nanofibers were immersed in laminin solution (10 mg/mL) (Sigma-Aldrich) overnight at 4 ºC. The remaining laminin solution was aspirated and the samples were washed with sterile water for 5 min, and then used immediately.

3.4 PLLA films and nanofibers Cell Adhesion assay

The capacity of cells to adhere to PLLA films and nanofibers was measured upon cell exposure to the biomaterials for 2h. Quantification of adherent cells was performed indirectly by scoring the number of non-adherent resuspended cells in the media. Briefly, $1x10^5$ cells cm^{-2} were seeded on PLLA films and nanofibers (random and aligned), uncoated or coated with Laminin, in 24-well plates. After 2h of incubation, cell media were collected and an aliquot applied to a haemocytometer. Non-adherent cells present in the cell media were counted using the Trypan blue assay and the number of viable non-adherent cells determined. Consequently, the percentage of adherent cells was calculated, taking the $1x10^5$ cells initially seeded as 100%. Two independent experiments were performed in triplicate and expressed as the mean ± standard error of the mean.

3.5 Biocompatibility assay

The resazurin metabolic assay was used to determine the biomaterials cytotoxicity/biocompatibility to SH-SY5Y cells. This bioassay measures the conversion of resazurin to resorufin by metabolically active cells, as it results in the generation of a fluorescent product proportional to the number of viable cells.

The approach here used involved seeding cells in 24-well cluster plates at $5x10^4$ cells cm^{-2} with the PLLA films and nanofibers (random and aligned), uncoated and coated with Laminin (Sigma-Aldrich). Then, at the indicated time points, cells were incubated for 4 h with fresh medium containing 10% of a resazurin (Sigma-Aldrich) solution (0.1 mg.mL^{-1} resazurin in phosphate buffer saline (PBS) [Pierce, Perbio, Thermo Scientific, Bonn, Germany]). Resazurin reduction was thereafter measured spectrophotometrically (Cary 50 BIO, Varian, Palo Alto, CA, USA or Infinite 200 PRO (Tecan)) at 570 and 600 nm. Two independent experiments were carried out in triplicate and expressed as mean ± standard error of the mean.

3.6 Cell morphology evaluation

Actin Staining

In order to visualize F-actin, a cytoskeleton filamentous protein, cells grown on coverslips, on PLLA films, and on nanofibers (random and aligned) were fixed with a 4% paraformaldehyde PBS solution for 20 min and washed three times with PBS. Cell permeabilization was accomplished with a 0,1% Triton PBS solution for 5 min, followed by three PBS washes. Then, the coverslips and

the materials were incubated for 20 minutes in the dark with Alexa Fluor 568 Phalloidin (Invitrogen) diluted (1:50) in PBS with 1% BSA. Coverslips, films and nanofibers (aligned and random) were further washed three times with PBS and one last time with distilled water, and then mounted with the DAPI-plus VECTASHIELD® mounting media (Vector Laboratories) on 0.1 mm microscope glass slides for epifluorescence and confocal microscopy analyses. Epifluorescence microscopy was carried out using an Olympus IX-81 motorized inverted microscope equipped with LCPlanFl 20x/0.40 objective lens. Confocal microscopy was performed with a LSM 510 META confocal microscope (Zeiss, Jena, Germany) using an Argon laser line of 488 nm (FITC channel), and a Diode 405-430 laser (DAPI channel).

3.7 Cell collection and protein content quantification

Upon the indicated time points, cells were harvested with the suitable volume of 1% boiling SDS. Cell lysates were then boiled for 10 min and sonicated for 30 sec. Total protein measurements were performed in an aliquot of the cell lysates using Pierce's BCA protein assay kit, following the manufacturer's instructions. This assay is based on the well-known reduction of Cu^{+2} to Cu^{+1} by protein in an alkaline medium, followed by a sensitive and selective colorimetric detection of the cuprous cation using bicinchoninic acid (BCA). Chelation of two molecules of BCA with one Cu^{+} ion gives origin to a purple-colored reaction product that is a water-soluble complex with a strong absorbance at 562 nm. The formation of the purple-colored product is proportional to the protein concentration over a working range of 20-2000 µg/ml. To determine the protein concentration of each sample, a standard curve was prepared in a microplate by plotting BSA absorbance vs. BSA standard concentration according to table 7.

Table 7 – Preparation of standards for the BCA protein assay. BSA - Bovine serum albumin (2 mg/ml).

Standards	BSA (µl)	1% SDS (µl)	Protein mass (µg)
P_0	-	25	0
P_1	1	24	2
P_2	2	23	4
P_3	5	20	10
P_4	10	15	20
P_5	20	5	40

Duplicates of each sample to be assayed were prepared in the microplate, taking 5 µl of each sample plus 20 µl of 1% SDS. 200 µl of working reagent (W.R.; mixture of BCA reagent A with BCA reagent B in the proportion of 50:1) was rapidly added to all the microplate wells (standards and samples) and these were incubated at 37 ºC exactly for 30 min. The microplate was cooled at RT and the absorbance of each well was immediately measured at 562 nm using the microplate reader Infinite 200 PRO (Tecan).

3.8 Western Blot analyses

Mass-normalized cell aliquots (according to BCA results) were subjected to electrophoresis on a 5-20% gradient sodium dodecylsulfate (SDS) polyacrylamide gel (SDS-PAGE), and subsequently transferred onto nitrocellulose membranes. After the electrotransfer of proteins, Ponceau S staining was used for the detection of total protein present on the nitrocellulose membrane, as it is a negative stain that reversibly binds to the positively charged amino groups of the protein and to non-polar regions in the protein. This staining technique is reversible and allowed further immunological detection [78]. After membranes were initially soaped in 1X TBS, they were incubated with Ponceau S Staining Solution for 5 min, and then rinsed with distilled water until the background was clear. Ponceau stained membranes were scanned using GS-800™ Calibrated Densitometer (Bio-Rad), for further loading corrections, and then immersed in a TBS-T 1x solution until protein bands disappear.

For immunological detection, firstly, possible non-specific binding sites of the primary antibody were blocked by immersing the membrane in 5% non-fat dry milk in 1X TBS-T solution for 1-2 h. Then the incubation with primary antibody was carried out for a period of time accordingly to the manufactures instructions (ranging from 2 h to overnight incubation). After three washes with 1X TBS-T of 10 min each, the membrane was further incubated with the appropriate secondary antibody for 2 h with agitation. Membrane was additional washed three times with 1X TBS-T for 10 min before being submitted to the enhanced chemiluminescence (ECL) detection method. This is a light emitting non-radioactive method used for the detection of immobilized specific antigens, conjugated directly or indirectly with horseradish peroxidase-labeled antibodies. Washed membranes were incubated for 1 min at RT with a homemade ECL detection solution or for 5 min with the Luminata™ Crescendo (Millipore) ECL solution. ECL detection solution in excess was drained. In a dark room, an autoradiography film was placed on the top of the membrane, inside a film cassette. The cassette was closed and the blot was exposed for an appropriate period of time. The film was then removed and developed in a

developing solution (Sigma Aldrich), washed in water, and fixed in a fixing solution (Sigma Aldrich). The membrane was further washed in TBS-T and distilled water before drying, for better conservation, while the resulting film was scanned with the GS-800™ Calibrated Densitometer. Band intensities were quantified using the Quantity One densitometry software (Bio-Rad) and then the obtained values were corrected for the relative Ponceau S (loading control) lane levels.

All primary and secondary antibodies used were diluted (specific dilutions in Table 8), accordingly to the manufactures instructions in a blocking solution of 1X TBS-T/3% non-fat dry milk or 1X TBS/3% BSA.

Table 8 - Antibodies used in the immunoblots: respective target protein, specific dilutions used and the objective for which the antibody was used in the context of the study. (All the secondary antibodies were from Amersham Pharmacia).

Target protein/ epitope	Primary antibody	Secondary antibody	Objective
Cleaved PARP	Anti-PARP cleavage site (Millipore) polyclonal antibody Dilution: 1:1000 in a TBS-T/3% BSA solution	Horseradish Peroxidase conjugated α-rabbit IgG Dilution: 1:5000 TBS-T/3% non-fat dry milk solution	Marker for detecting apoptosis
Actin	Monoclonal Antibody to Actin (pan) (Acris) Dilution: 1:10 in TBS-T/3% non-fat dry milk	Horseradish Peroxidase conjugated α-mouse IgG Dilution: 1:5000 TBS-T/3% non-fat dry milk solution	Detection of cytoskeleton remodeling
β-Tubulin	2-28-33 (Invitrogen) Dilution: 1:2000 in TBS-T/3% non-fat dry milk	Horseradish Peroxidase conjugated α-mouse IgG Dilution: 1:5000 TBS-T/3% non-fat dry milk solution	

3.9 Differentiation of the SH-SY5Y cell line

To evaluate the potential of PLLA nanofibers (random and aligned) to facilitate differentiation, SH-SY5Y cells were differentiated by incubation with 10 µM Retinoic Acid (RA) in 10% FBS medium for ten days, with RA being added every other day, and cell medium replaced at that time. After PLLA samples UV sterilization, cells were seeded on uncoated PLLA nanofibers (random and aligned) in 12-well cluster plates at 5×10^4 cells cm^{-2}. After 2 days in culture, cells grown on coverslips and on PLLA nanofibers were stained for F-actin as described in section 3.61.

3.10 Neuronal primary culture on aligned nanofibers

Primary rat neuronal (cortical) cultures were carried out to evaluate the differences in neuronal differentiation. Cerebral cortex was dissected from Wistar Hannover rat embryos at 18th day of gestation. Cortical cultures were dissociated with trypsin (0.23 mg/ml), and deoxyribonuclease I (0.15 mg/ml) in Hanks balanced solution (HBSS). Cells were washed with HBSS supplemented with 10% FBS to stop trypsinization, centrifuged at 1000 rpm for 2 minutes, and further washed and centrifuged with HBSS for serum withdraw. Cells were plated onto poli-D-lysine coated coverslips and PLLA samples at a density of $4,0 \times 10^5$ cells/cm^2 in a 12-well plate and cultured for 10 days in Neurobasal medium (Gibco) supplemented with 2% B27 (final concentration), a serum-free medium combination. The medium was further supplemented with glutamine (0.5 mM), gentamicin (60 µg/ml), and glutamate (25 µM). Cells were maintained in an atmosphere of 5% CO_2 at 37°C and monitored in an inverted optical microscope.

Immunocytochemistry analyses of neuronal cultures

After 3 days in culture (stage 3), cells were fixed and permeabilized as in 3.6.1 section. Cells were then incubated with an anti-βIII tubulin (alias Tuj-1) primary antibody (1:200 in PBS 3% BSA) for 2 h at RT. The antibody was removed by washing 3 times with PBS and a solution of PBS 3% BSA containing Alexa Fluor 568 Phalloidin (1:50) and the specific secondary antibody – Alexa Fluor 488 (1:300) was added to coverslips and to PLLA samples. After 3 washes with PBS and one with deionized water, coverslips and materials were mounted with DAPI-plus VECTASHIELD® reagent on glass slides for epifluorescence (Olympus IX-81) and confocal microscopy analyses (LSM 510 META confocal microscope with an Argon laser line of 488 nm (FITC/Alexa 488 channel), a Diode 405-430 laser (DAPI channel) and 561 nm DPSS laser (Alexa 568 channel).

Cell counts and neurite length measurements were performed using the ImageJ freeware. Cells positive for βIII tubulin were considered differentiated neurons, as this is a neuron specific marker, and βIII tubulin-positive neurites were measured using the NeuronJ plugin of ImageJ.

3.11 Protein identification and quantification by nano-HPLC-MALDI-TOF/TOF

Mass-normalized cell aliquots (according to BCA results) were subjected to electrophoresis on a 5-20% gradient SDS-PAGE. The resulting gel was incubated with the Brilliant Blue G (Sigma) staining solution for 20 min to visualize bands and then washed with the distaining

solution ON until the background was clear. Afterwards, bands of interest were cut out of the gel using a sterile scalpel and kept at -20ºC while waiting for further analysis.

Protein bands excised manually from SDS-PAGE gel were destained with 25 mM ammonium bicarbonate/50 % acetonitrile and dried under vacuum (SpeedVac®, Thermo Savant, USA). The dried gel pieces were rehydrated with 25 μL of 10 μg/mL trypsin (Promega V5111) in 50 mM ammonium bicarbonate and digested overnight at 37 °C. Tryptic peptides were extracted from the gel with 10 % formic acid/ 50 % acetonitrile, dried in a vacuum concentrator and re-suspended in 10 μL of a 50 % acetonitrile/0.1 % formic acid solution. Separation of tryptic peptides by nano-HPLC was performed on the module separation Ultimate 3000 (Dionex, Amsterdam) using a capillary column (Pepmap100 C18; 3 μm particle size, 0.75 μm internal diameter, 15 cm in length). A gradient of solvent A [water/acetonitrile/trifluoroacetic acid (98:2:0.05, v/v/v)] to solvent B [water/acetonitrile/trifluoroacetic acid (10:90:0.045, v/v/v)] was used. The separation of 2 μg/μL sample was performed using a linear gradient (5-50% B for 30 minutes, 50-70% B for 10 minutes and 70-5% A for 5 minutes) with a flow rate of 0.3 μL/ minute. The eluted peptides were mixed with a continuous flow of α-CHCA matrix solution (270 nL/min, 2 mg/mL in 70% ACN/0.1% TFA and internal standard Glu-Fib at 15 ftmol) and applied directly on a MALDI plate in 7 seconds fractions using an automatic fraction collector Probot (Dionex, Amsterdam).

Mass spectra were obtained on a matrix-assisted laser desorption/ionization–time-of-flight MALDI-TOF/TOF mass spectrometer (4800 Proteomics Analyzer, Applied Biosystems, Foster City, CA, USA) in the positive ion reflector mode and obtained in the mass range from 700-4500 Da with 900 laser shots. Glu-Fib was used for internal calibration. A data-dependent acquisition method was created to select the 16 most intense peaks in each sample spot (considering 2 spots per fraction) for subsequent tandem mass spectrometry (MS/MS) data acquisition, excluding those from the matrix, due to trypsin autolysis or acrylamide peaks. A fragmentation voltage of 2kV was used throughout the automated runs. The spectra were processed and analyzed by the T2S (v1.0, Matrix Science Ltd, U.K.) and submitted in Mascot software (v.2.1.0.4, Matrix Science Ltd, U.K.) for protein/peptide identification based on MS/MS data using the following criteria: trypsin as enzyme; a maximum of two missed cleavages; mass tolerances of 20 ppm for peptide precursors, mass tolerance of 0.3 Da was set for fragment ions. Protein identifications based on MS/MS data were considered as reliable when the Mascot ion score confidence level for each individual peptide was higher than 32. The local FDR was calculated by searching the spectra against SwissProt (*Homo sapiens*, release date 01052013)

decoy (random) database. Quantification was performed using exponentially modified protein abundance index (emPAI) values, which is based on equation [79]:

$$emPAI = 10^{\frac{N_{observed}}{N_{observable}}} - 1$$

where 'N observed' is the number of experimentally observed peptides and 'N observable' is the calculated number of observable peptides, for each protein. Normalization to the total number of peptides in the sample was also performed.

3.12 Data analysis

Data is expressed as mean ± SEM (standard error of the mean) of the different experiments. Statistical significance analysis was conducted by one way analysis of variance (ANOVA) followed by the Tukey's test (SEM statistically different) or Welch's test (SEM non-statistically different).

4. Results

4.1 Effects of PLLA samples on cell adhesion

To assess the influence of PLLA samples on SH-SY5Y cell adhesion, the number of cells that did not adhere after 2h of culture onto empty plates or onto coated or uncoated non-polarized samples were measured using the Trypan blue assay (section 3.2). Figure 9 shows the percentage of adherent cells, calculated upon subtraction of the fraction of non-adherent cells (number of non-adherent cells divided by the total number of seeded cells).
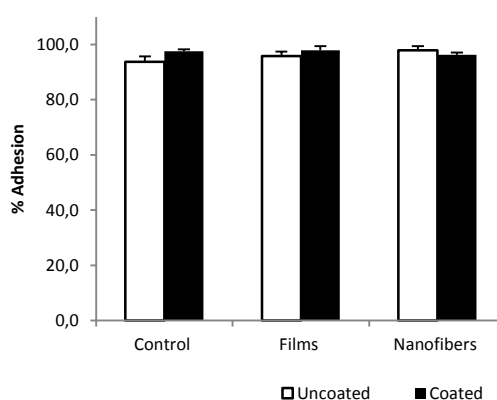
Figure 9 - Cell adhesion assay of SH-SY5Y cells seeded on PLLA films and nanofibers. $1x10^5$ cells were seeded in 24 well plates containing the polymers, uncoated or coated with laminin. n = 6

According to these results, cell adhesion does not vary when SH-SY5Y cells are seeded onto the PLLA samples. Furthermore, even the laminin-coating does not improve the ability of SH-SY5Y cells to adhere to the plastic plate or to the PLLA samples.

4.2 Effects of PLLA samples on cell viability

Cell viability and proliferation of SH-SY5Y cells cultured for 2, 5, 8 and 11 days on non-polarized and polarized PLLA films and nanofibers were evaluated by the non-destructive and non-toxic resazurin metabolic assay. Results are shown in figure 10.
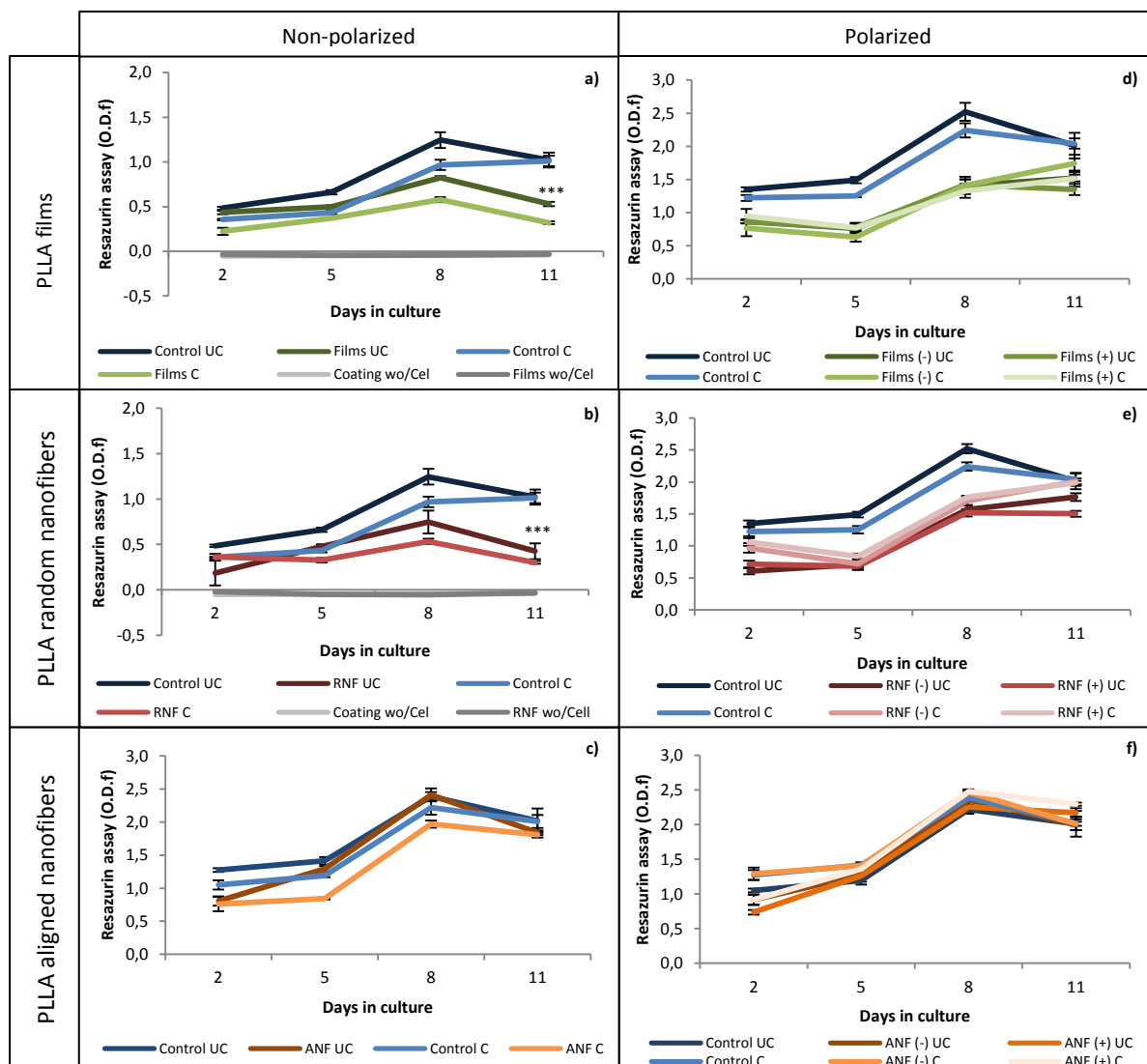
Figure 10 – Resazurin cell viability assay of SH-SY5Y cells exposed to PLLA films and nanofibers for 11 days. a), b) and **c)** represent the effects of non-polarized PLLA films, random, and aligned nanofibers on cell viability, respectively. **d), e)** and **f)** represent the effects of negatively (-), positively (+) polarized PLLA films, random, and aligned nanofibers on cell viability, respectively. *UC – Uncoated; C – Laminin - coated; wo/Cell – plates only coated or only with the materials, without cells, RNF – random nanofibers, ANF – aligned nanofibers.* Results are presented as Resazurin $O.D._F$ mean ± SE, n = 6. *** ($p < 0,001$) statistically significant differences between films and nanofibers when compared to control, both in coated and uncoated conditions at the 11th day.

Since there were no significant differences in the adhesion assay it can be assumed that the cell viability assay started with the same number of cells for the different conditions under analysis. Thus, any differences between experimental conditions are, most likely, due to their effects on cells viability (proliferation and death), rather than dissimilarities in initial cell adhesion to the material. Furthermore, from the analysis of the negative controls of Figure 10 (*Coating wo/Cell, Films wo/Cell, Nanofibers wo/Cell*), neither the materials (PLLA films and nanofibers) nor the laminin coating interfered with the resazurin assay, as their $O.D._F$ is approximately zero.

The viability/proliferation assay in figure 10 shows that the PLLA samples are probably not cytotoxic to SH-SY5Y cells, as the number of cells at the end of the assay is not lower than the initial number of seeded cells. However, some relevant differences in proliferation are observed between control cells, films and nanofibers, and between coated and uncoated conditions.

In general, the growth curves of cells cultured directly on the well (control UC and control C) are similar to the ones of cells cultured on the materials, increase until 8 days in culture and then maintain or slightly decline until the 11th day, yet the amplitudes of the curves differ. The coating with laminin normally reduces the number of viable cells, not only for the control conditions, but also for the non-polarized PLLA samples. For cells grown in uncoated conditions, the number of viable cells cultured on the control well, on non-polarized PLLA films (figure 10a), or on random nanofibers (figure 10b) is, firstly similar (day 2), but with time in culture the number of control viable cells increase more than in other conditions. These results indicate that cells proliferate more when they are cultured in the absence of these materials. However, analyzing the graph in figure 10c, we can see that non-polarized PLLA aligned nanofibers induce this effect only at an earlier phase (day 2), with this difference relatively to the number of control cells being annulated (uncoated) or diminished (coated) from 5 days on.

Polarization of PLLA samples also produces alterations in the number of cells in comparison to control, however there are no significant differences between negatively and positively polarized samples. Polarized PLLA films (figure 10d) and nanofibers (figure 10e) accentuated the decrease in the number of viable cells seen in their non-polarized counterparts (figures 10a and 10b, respectively). Nonetheless, this seems only a delay in the cell proliferation rate since at the 11th day cell viability on polarized films and random nanofibers approaches control conditions. On the other hand, polarized PLLA aligned nanofibers (figure 10f) did not affect proliferation, as the growth curves of control and tested conditions coincide. Of note, laminin coating had few or none effect on the growth curve of cells grown on polarized samples.

In conclusion, there is a decrease in the proliferation rate when cells are cultured on PLLA samples, except for PLLA aligned nanofibers, particularly when polarized. To assess if this effect occurs due to an induction of apoptosis, cleaved Poly (ADP-ribose) polymerase (PARP) levels were measured in cells lysates at the 11th day. PARP in its full length (116 KDa) is a crucial protein that regulates the cell cycle, DNA repair and genomic stability. However, during apoptosis, PARP is cleaved by caspase 3 and 7 and yields two fragments: 85KDa and 25KDa fragment [80]. Thus, the levels of cleaved PARP at the last incubation time point (11 days) were measured to evaluate the yield of apoptotic cells, with the results obtained being shown in figure 11.
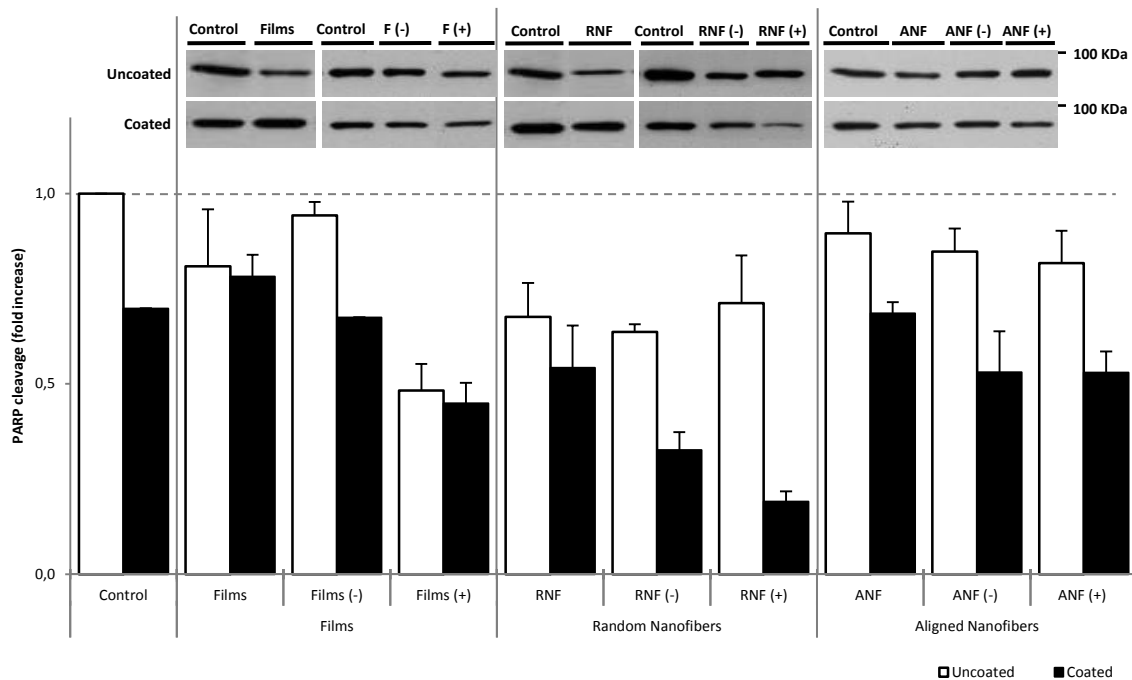
Figure 11 - Effects of PLLA polymers on apoptosis. Immunoblot analysis of SH-SY5Y cells lysates after 11 days in culture with PLLA polymers – films, random and aligned nanofibers, either non-polarized, negatively (-) and positively (+) polarized, uncoated or laminin coated. Cellular levels of cleaved PARP were detected using a primary antibody cleavage site-specific antibody to the 85 KDa fragment of PARP. The bottom graph represents the variation (fold increase over uncoated control cells) of cleaved PARP levels with different culture conditions. Data was normalized using Ponceau staining as loading control. *F, films; RNF – random nanofibers; ANF – aligned nanofibers*. Mean ± SE, n=2

Results presented in figure 11 clearly show that PLLA samples do not induce cell apoptosis as cleaved PARP levels decrease in all experimental conditions. Nevertheless, there are some significant variations of cleaved PARP levels among control and experimental conditions. Coating with laminin reduces cleaved PARP levels by ~30%. PLLA films almost do not affect (non-polarized or negatively polarized), or reduce cleaved PARP levels by ~ 50% (positively polarized PLLA films). The decrease of cleaved PARP levels is more accentuated when cells are cultured on PLLA random nanofibers (~30%, as the coating effect) than for cells cultured on PLLA aligned nanofibers. Polarization of nanofibers (random or aligned) *per se* has less influence on these decreases, but associated with coating it enhances the decrease in cleaved PARP levels. This is particularly evident for the random nanofibers. In synthesis, these results indicate that the decrease of cell viability does not result from an induction of apoptosis.

4.3 Effects of non-polarized PLLA samples on cell morphology

Morphology of SH-SY5Y cells cultured on the materials for 11 days was monitored by fluorescence microscopy (figure 12) in order to examine any alterations in cell architecture and to visualize the cell cytoskeleton, more specifically F-actin, a fundamental cytoskeleton protein.

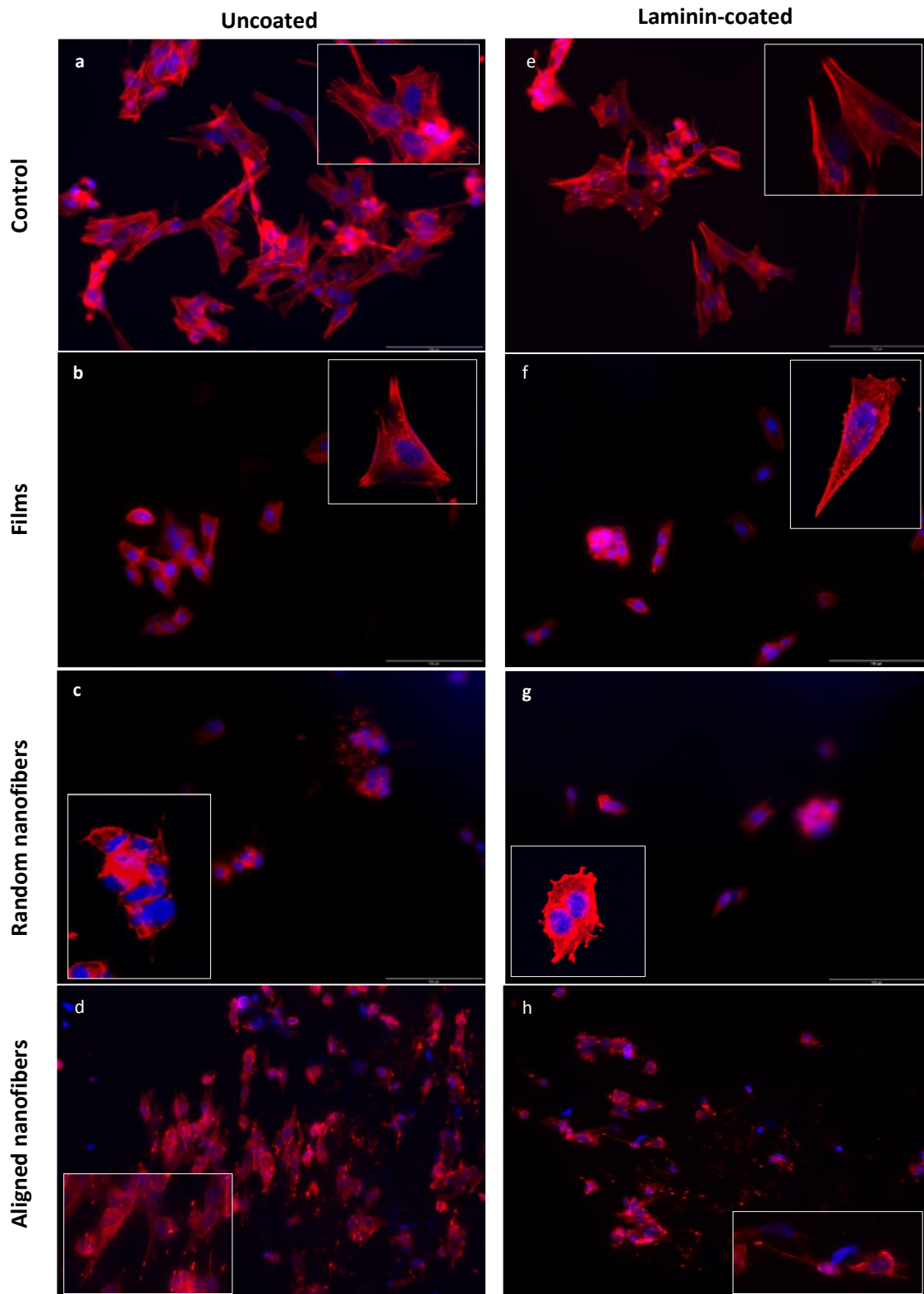**Uncoated** **Laminin-coated**

Figure 12 – Fluorescent and confocal microscopy analysis of SH-SY5Y cells grown on uncoated and laminin-coated PLLA samples for 11 days. F-actin is visualized in red upon staining with Alexa Fluor 568 Phalloidin. Nuclei are visualized in blue upon DAPI staining. Bar = 100 µm.

The analysis of figure 12 reveals dramatic alterations in cell number and shape and rearrangements in cytoskeleton dynamics when cells are cultured on PLLA samples. Concerning the number of cells, it is evident a decrease in the number of cells when culture is performed on PLLA samples, except for cells cultured on aligned PLLA nanofibers. In addition, coating with laminin also decreases the number of cells by itself and further decreases the number of cells on the materials. These results are in agreement with cell viability assay results, since it was seen a decrease in cell proliferation rate upon cell culture on PLLA films and random nanofibers, while PLLA aligned nanofibers does not affect the number of viable cells at the end of the experiment. Looking at figure 12 it is also evident an alteration in SH-SY5Y cell shape when cells are cultured with PLLA samples. The flat topography of PLLA films preserves the "natural" cuboid morphology of SH-SY5Y cells, while PLLA random nanofibers meshes transforms SH-SY5Y cells into a round-shaped cells prone to aggregate. PLLA aligned nanofibers, in contrast, do not induce cell-cell aggregation, and create a mixed phenotype, in which some cells present a rounded morphology and others present a more elongated morphology, with similar "neurite-like projections" as control cells.

These alterations in cell shape can be attributed to alterations in cytoskeleton dynamics observed in figure 12 through F-actin staining. In comparison to uncoated control, laminin-coating cultured cells present a reduction in the organization of F-actin in the form of stress fibers. PLLA films cultured cells also induce the same effect in addition to an increase of F-actin cortical distribution and actin depolymerization. Cells cultured on PLLA nanofibers completely lose stress fibers and an increase F-actin depolymerization arises. Nonetheless, while random nanofibers induce F-actin depolymerization and retract "neurite-like projections", nanofibers alignment potentiates the maintenance of these extensions that seem to align along the substrate.

The main findings about the SH-SY5Y cell number, size, shape, and spreading as well as actin cytoskeleton-related information upon culture on the different PLLA samples are summarized in Table 9. Actin distribution is divided in three phenotypes: *Fibers* - a fibrous phenotype where cells show mainly long actin stress fibers that cross the entire cell; *Cortical* – a cortical phenotype, where disorganization of actin fibers within the cell body and clumping of F-actin at the periphery, beneath the plasma membrane, is visible; *Intermediate* - shows less stress fibers and some spots of smaller F-actin polymers within the cell body [81].

Table 9 - Morphometric data obtained from the analysis of cells cultured on films and nanofibers (as in figure 12a, b, c, d, e, f, g and h).

Condition		Number of cells	Cell size	Cell shape	Cell spreading	F-Actin stress fibers	Actin distribution
Control	Uncoated	+++	Normal	Cuboid	Spread	+++	Fibers
	Laminin - coated	++	Normal	Cuboid	Spread	++	Fibers
PLLA films	Uncoated	++	Small	Cuboid	Spread	++	Fibers
	Laminin - coated	+	Small	Cuboid	Spread/aggregated	+	Intermediate
PLLA random nanofibers	Uncoated	+/-	Very small	Round	Aggregated	-	Cortical
	Laminin- coated	+/-	Very small	Round	Spread/aggregated	-	Cortical
PLLA aligned nanofibers	Uncoated	+++	Normal/ small	Cuboid / round	Spread	-	Cortical
	Laminin - coated	++	Small	Cuboid / round	Spread	-	Cortical

These results indicate that PLLA samples induce dramatic morphological alterations in SH-SY5Y cells. Since cell architecture is defined by its cytoskeleton, actin and β-tubulin levels were evaluated and the results obtained are presented in figure 13.
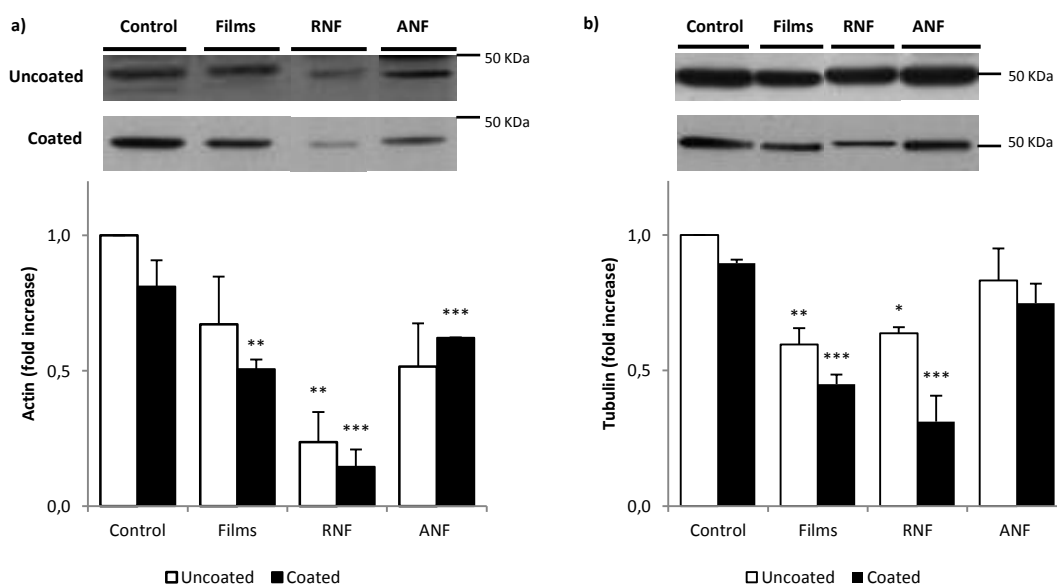
Figure 13 – Effects of non-polarized PLLA samples on cytoskeleton levels. Immunoblot analysis of **actin and tubulin levels in** SH-SY5Y cells cultured for 11 days on non-polarized PLLA polymers (films, random and aligned nanofibers). Cellular levels of **a)** actin and **b)** β-tubulin were detected using specific antibodies for actin (42 KDa) and β-tubulin (50 KDa). The bottom graphs represent the variations (fold increase over uncoated control cells levels) of actin and β-tubulin levels with different culture conditions. Data was normalized using Ponceau staining as loading control. *RNF – random nanofibers, ANF – aligned nanofibers*. Mean ± SE, n=3. * (*p < 0,05*) ** (*p < 0,01*) *** (*p < 0,001*)

The results indicate that laminin coating slightly decreases actin (figure 13a) and β-tubulin (figure 13b) levels (by ~10%), with this decreases being much more accentuated upon SH-SY5Y cell culture on PLLA samples. PLLA films reduce actin levels by ~30% and β-tubulin by ~40%. Culture on PLLA random nanofibers produces the most significant alteration in actin levels (reduction by ~75%), while for β-tubulin levels PLLA random nanofibers induce a less prominent decrease (~35%), similar to β-tubulin levels of cells cultured with PLLA films. Laminin-coating of PLLA films and random nanofibers further decrease actin and β-tubulin levels by ~10-20%, except for β-tubulin of cells grown onto random nanofibers, where coating induces a further ~35% decrease. Cells cultured on PLLA aligned nanofibers present actin and β-tubulin levels distinct from random nanofibers: actin levels decrease by ~40-50% independently from coating; the decrease of β-tubulin levels is less noticeable, being only ~10% over control. Taken together, these results indicate that cells cultured with PLLA random nanofibers are subjected to more pronounced actin-cytoskeleton alterations, consistent with the morphological alterations observed in figure 12.

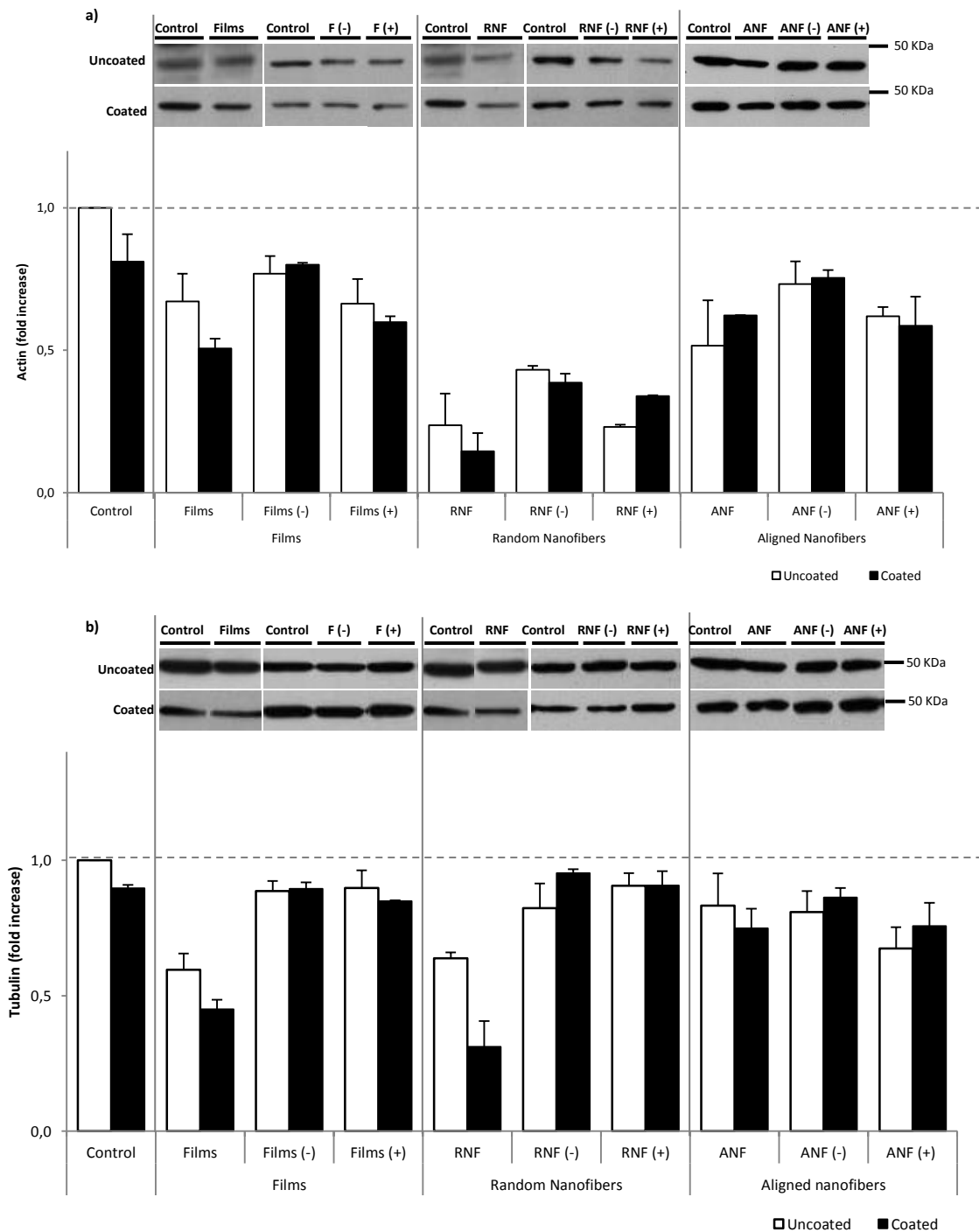## 4.4 Effects of polarized PLLA samples on cell morphology

In order to study the influence of polarization on SH-SY5Y cell morphology, F-actin staining was performed for cells cultured on polarized PLLA samples (figure 14).

Results show that polarized PLLA samples produce significant alterations in cell morphology and distribution on the substrate in comparison to control (cells without materials) and with their non-polarized counterparts. In comparison to non-polarized PLLA films (figure 14a and b), negatively and positively PLLA films induce an increase in cell spreading. Furthermore, it seems that laminin-coating enhance this effect in positively polarized PLLA films. Concerning cells cultured on polarized PLLA nanofibers, it is evident that this substrate causes a high amount of cell aggregation, besides the complete loss of stress fibers observable in non-polarized PLLA nanofibers. Nevertheless, there are some subtle differences between cells cultured on random and aligned nanofibers. The spherical cell aggregates produced on PLLA random nanofibers are more confined (less cell spreading) than the ones formed on PLLA aligned nanofibers. Further and as for PLLA films, positive polarization of PLLA nanofibers together with laminin-coating favors cell spreading in the substrate (figure 14g and k), and this is even enhanced when cells are grown on aligned fibers (figure 14k). In relation to cytoskeleton dynamics, polarized films induce an increase of stress fibers formation and a decrease in actin depolymerization. PLLA nanofibers, on the other hand do not induce dramatic cytoskeleton alterations, comparing to their non-polarized equivalents.
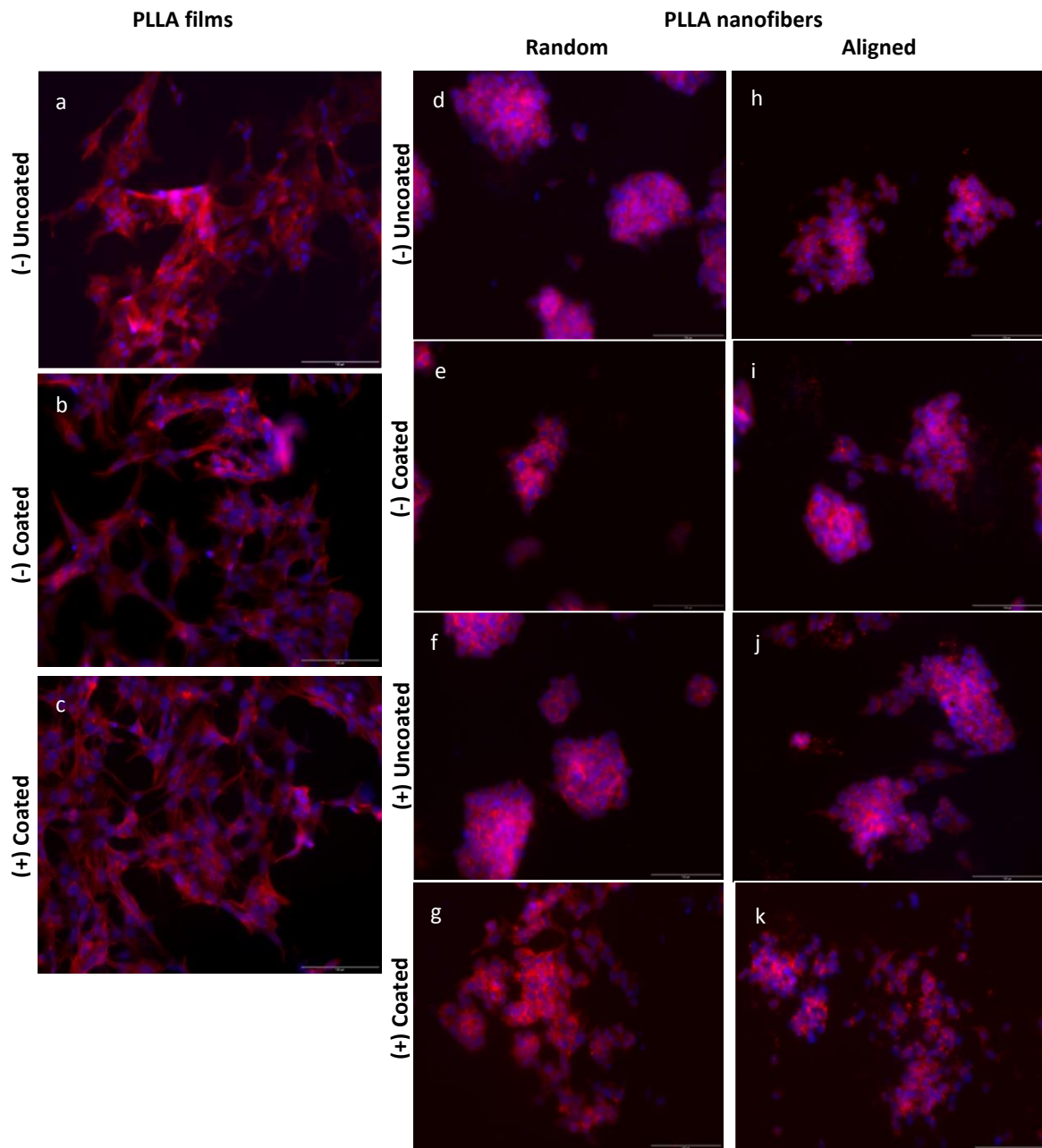
Figure 14 - Fluorescent microscopy analysis of SH-SY5Y cells exposed to polarized uncoated and laminin-coated polymers – PLLA films and nanofibers for 11 days. F-actin is visualized in red upon staining with Alexa Fluor 568 Phalloidin. Nucleus is visualized in blue upon DAPI staining. (+) uncoated microphotographs are absent since a technical problem occurred during fixation. Bar = 100 μm.

The same quantitative analysis of actin and β-tubulin levels was thus conducted to examine the alterations of cell cytoskeleton induced by PLLA samples polarization (figure 15).

Figure 15 – Effects of polarized PLLA samples on cytoskeleton levels. Immunoblot analysis of actin and beta-tubulin levels in SH-SY5Y cells after 11 days in culture on negatively (-) and positively (+) polarized PLLA samples (films, random and aligned nanofibers). Cellular levels of **a)** actin and **b)** tubulin were detected using specific antibodies for actin (42 KDa) and β-tubulin (50 KDa). The bottom graphs represent the variations (fold increase over uncoated control levels) of actin and β-tubulin levels with different culture conditions. Data was normalized using Ponceau staining as loading control. F – Films, *RNF – random nanofibers, ANF – aligned nanofibers.* Mean ± SE, n=2.

The overall analysis of figure 15 reveals that, as their non-polarized counterparts, all polarized samples also decrease actin levels over the control. However, in comparison to their non-polarized counterparts, in general, negatively polarized PLLA samples increase actin levels (figure 15a), while positively polarized PLLA samples maintain approximately the same actin levels. In its turn, coating with laminin slightly increases actin levels or maintains the same levels of uncoated polarized PLLA samples. Regarding to tubulin levels there is an increase of ~20% over non-polarized samples on polarized PLLA polymers, although polarized PLLA aligned nanofibers maintain the same levels of control and non-polarized samples. Furthermore, laminin-coating does not decrease tubulin levels as it occurred for non-polarized samples. In synthesis, polarization reverts the decrease in tubulin levels almost to control levels, and negative polarization partially reverts the decrease in actin levels.

4.5 Effects of polarized samples on neuron-like differentiation

So far, our results indicate that cells cultured on PLLA samples suffer dramatic cytoskeleton alterations that are not sufficient to trigger neuronal-like differentiation but that could be permissive to such alterations. Thus, our next step was to assess if these materials potentiate cell differentiation when an extracellular cue is added to cells.

To induce a neuron-like differentiation of SH-SY5Y cells a well-known morphogen – Retinoic Acid (RA) – was used [82]. After 2 in culture with 10 µM of RA, cells were fixed and F-actin was stained using Phalloidin. Figure 16 shows the results obtained.

Figure 16 reveals that, with only 2 days of differentiation a different morphological phenotype of SH-SY5Y cells is observed. In the presence of RA, control cells are smaller in size and present a higher number of processes ("neurite-like projections") arising from the cell body (compared with figure 12). Cells grown on PLLA nanofibers still occupy less space on the visible microscopy field, not only because they are smaller, but also because they seem to proliferate less. Although SH-SY5Y cells still tend to form aggregates in this experimental set-up, these are again smaller in PLLA aligned nanofibers. With respect to differentiation, cells differentiating on aligned nanofibers, non-polarized and polarized, and on random positive nanofibers appear to possess a higher number of "neurite-like projections". Further, these cells possess more elongated "neurite-like projections" than control differentiating cells, and these projections align along the nanofibers. Lastly, our results suggest that positive polarization and fibers alignment favor the increase of neurite length.
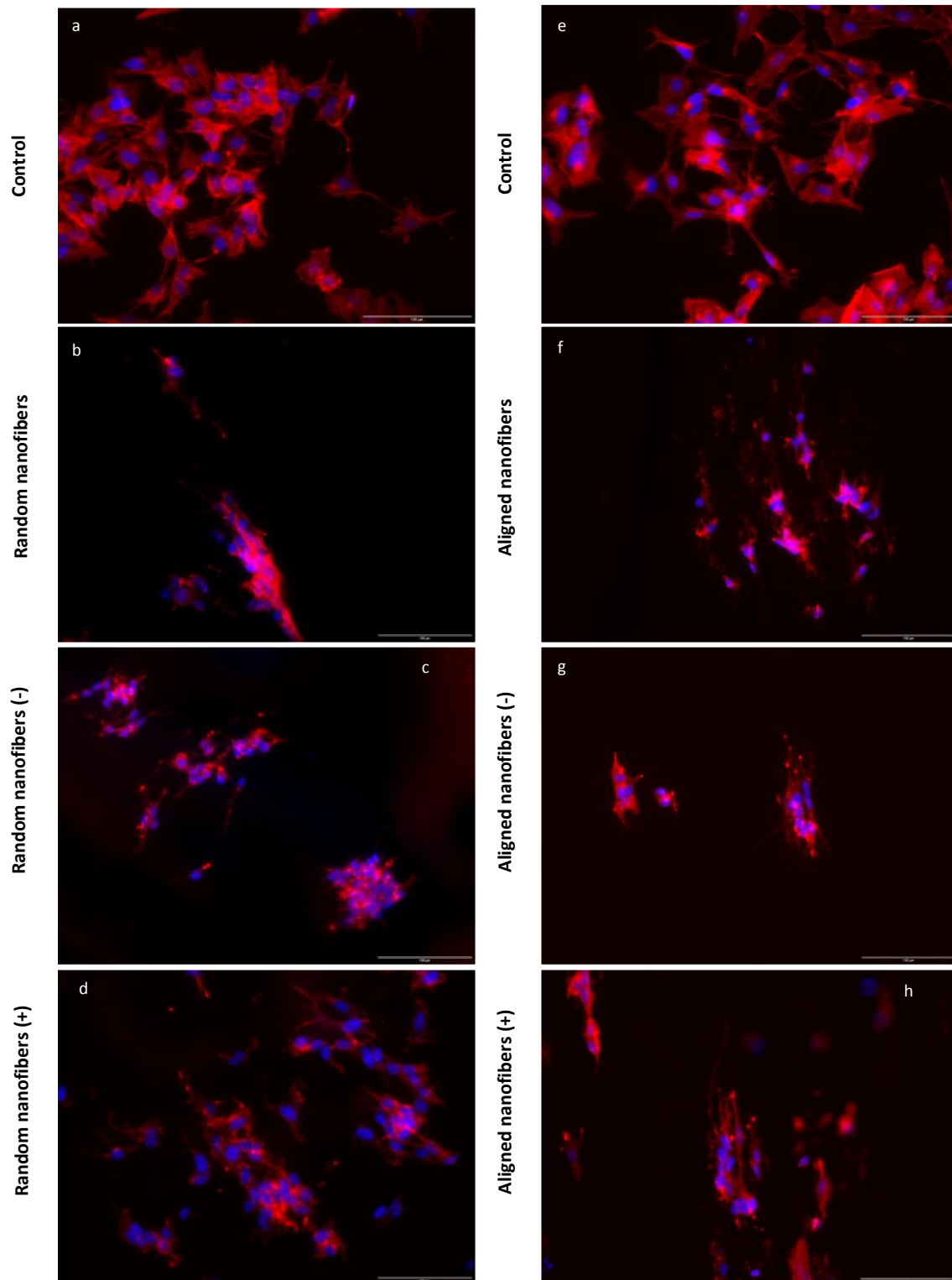
Figure 16 - Fluorescent microscopy analysis of SH-SY5Y cells exposed to 10 μM of Retinoic acid and cultured on polarized PLLA nanofibers for 2 days. F-actin is visualized in red upon staining with Alexa Fluor 568 Phalloidin. Nuclei are visualized in blue upon DAPI staining. Bar: 100 μm.

4.6 Effects of polarized PLLA samples on neuritic outgrowth

From the analysis of figure 16, PLLA aligned nanofibers are the polymers that produce better enhancement on neuritic length. Thus, this polymer form was further challenged in primary embryonic cortical neuronal cultures at 3 days (figure 17), when, it is already visible, a longer neurite that corresponds to the "growing" axon and dendrites are elongating.
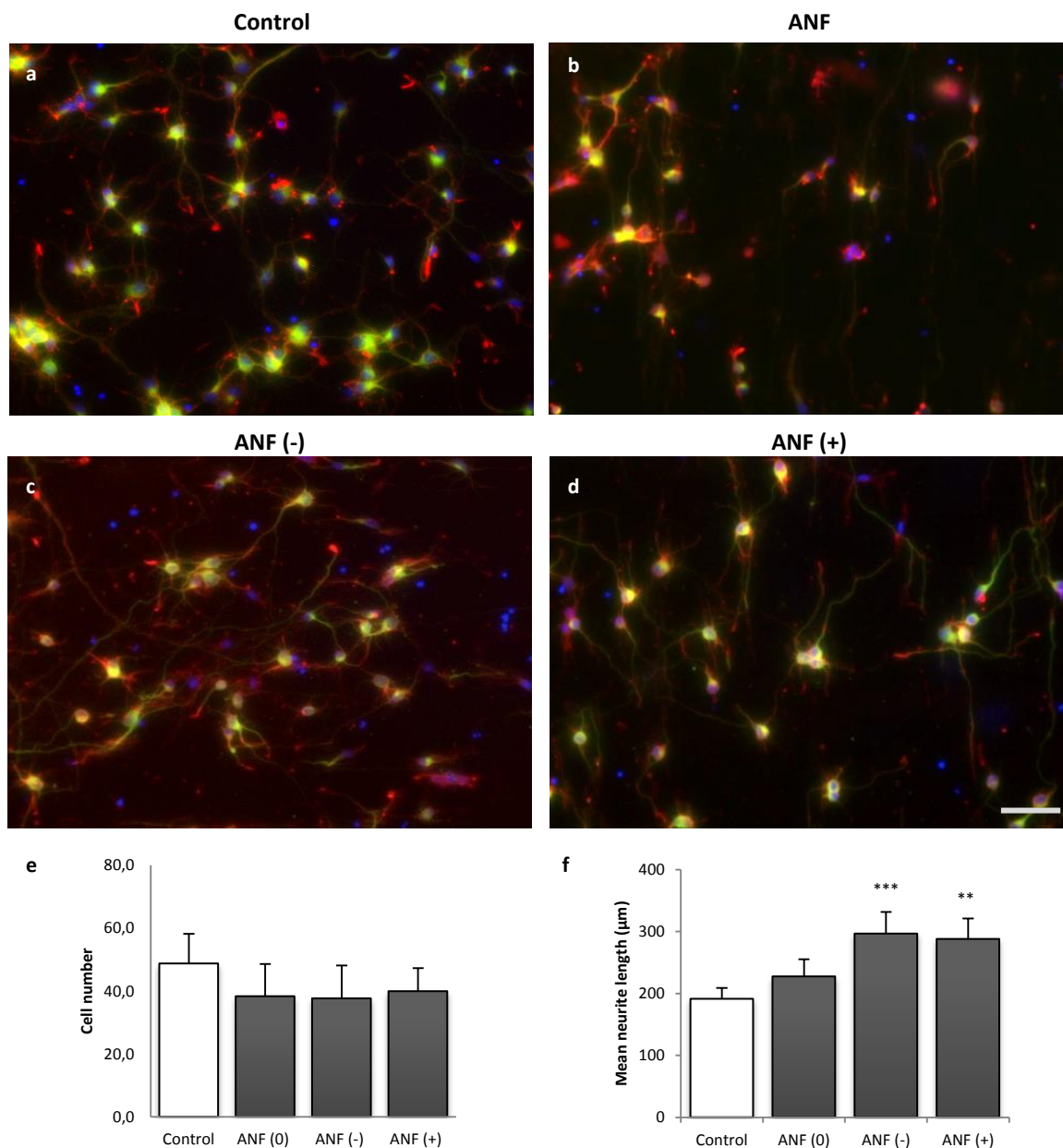
Figure 17 - Fluorescent microscopy analysis of embryonic cortical primary neurons cultured on PLLA aligned nanofibers for 3 days. (a, b, c, d) F-actin is visualized in red upon staining with Alexa Fluor 568 Phalloidin. β-III tubulin is visualized in green upon incubation with a primary antibody specific for this neuron-specific cytoskeletal protein, and an Alexa Fluor 488-conjugated secondary antibody. Nuclei are visualized in blue upon DAPI staining. **(e)** Average of cell counting from 10 random microscopic fields using the *cell counter* plugin of ImageJ. **(f)** Mean of neuritic length measured in β-III tubulin channel using the neuron plugin of ImageJ n=60. Bar = 100 μm. ** ($p < 0,01$); *** ($p < 0,001$).

These results show that although there is a slight decrease in cell number (figure 17 e), it is not statistically significant. Importantly, differences are observed in the neuritic length (figure 17f). Besides the general increase in neurite length when neurons were cultured on PLLA aligned nanofibers, polarization highly enhances this effect, although the orientation of neurites along nanofibers is, apparently, lost in negatively polarized PLLA aligned nanofibers.

4.7 Proteomic analysis

While performing Ponceau staining, differences in some bands total protein content between control and PLLA samples became evident (see figure 18).
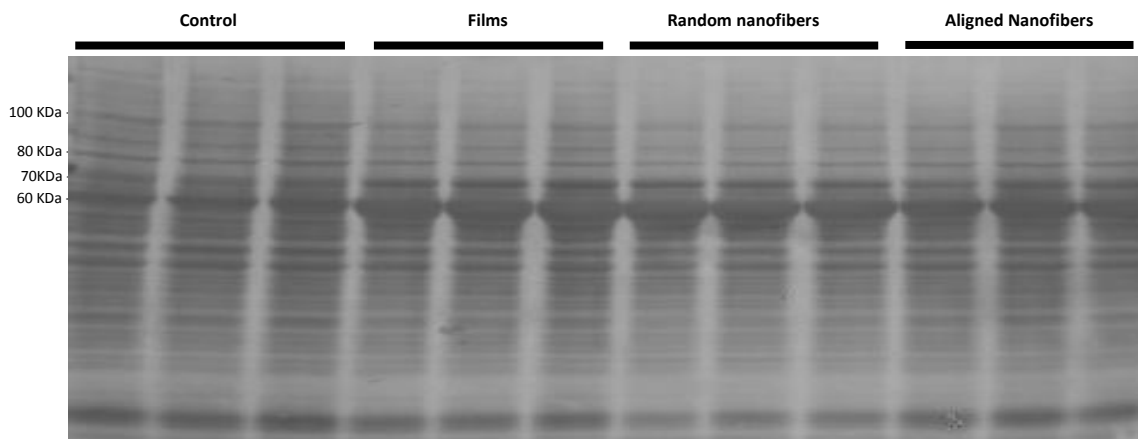
Figure 18 - Ponceau staining of total protein bands on the membrane.

Alteration of protein content was more pronounced around 100, 80, 70, and 60 KDa. Around 100 and 80 KDa a decrease of band intensity, in relation to control, is visible in cells culture on the samples; additionally, random nanofibers seem to produce the most significant decrease. Conversely, around 70 and 60 KDa an increase of band intensity, in relation to control, is visible in cells cultured on the materials; again random nanofibers seem to produce the most significant increase. As random nanofibers presented the highest degree of alteration, this polymer was chosen for mass spec analysis. Thus, after Comassie blue staining, the bands of interest were extracted from two samples of the random nanofibers and submitted to mass spec processing in order to identify the proteins whose levels were altered in cells cultured on PLLA nanofibers (summarized in table 10, extended in appendix, table 13).

Table 10 – Summary of proteins identified through mass spec analysis in SH-SY5Y cells cultured on nanofibers (n=2). Protein expression was considered altered if: Mascot score > 32. '*Unique*' - proteins found in both samples of only one condition (control or PLLA nanofibers); '*Upregulated*' - proteins whose normalized emPAI value is superior in duplicates of the same condition (control vs PLLA nanofibers). '*Total*'- the number of unrepeated proteins.

Band	Identified proteins	Proteins with different expression levels			
		Control		PLLA nanofibers	
		Unique	Upregulated	Unique	Upregulated
100 KDa	53	2	4	4	0
80 KDa	45	4	2	1	3
70 KDa	59	2	2	6	2
60 KDa	46	5	0	1	5
Sum	203	13	8	12	10
		43			
Total	117	37			

From a total of 117 different proteins, 37 were expressed differently when cultured on PLLA random nanofibers. The function of these proteins was first assessed using the PANTHER (Protein ANalysis THrough Evolutionary Relationships) Classification System [83]. Figure 19 shows a summary of identified protein biological processes.
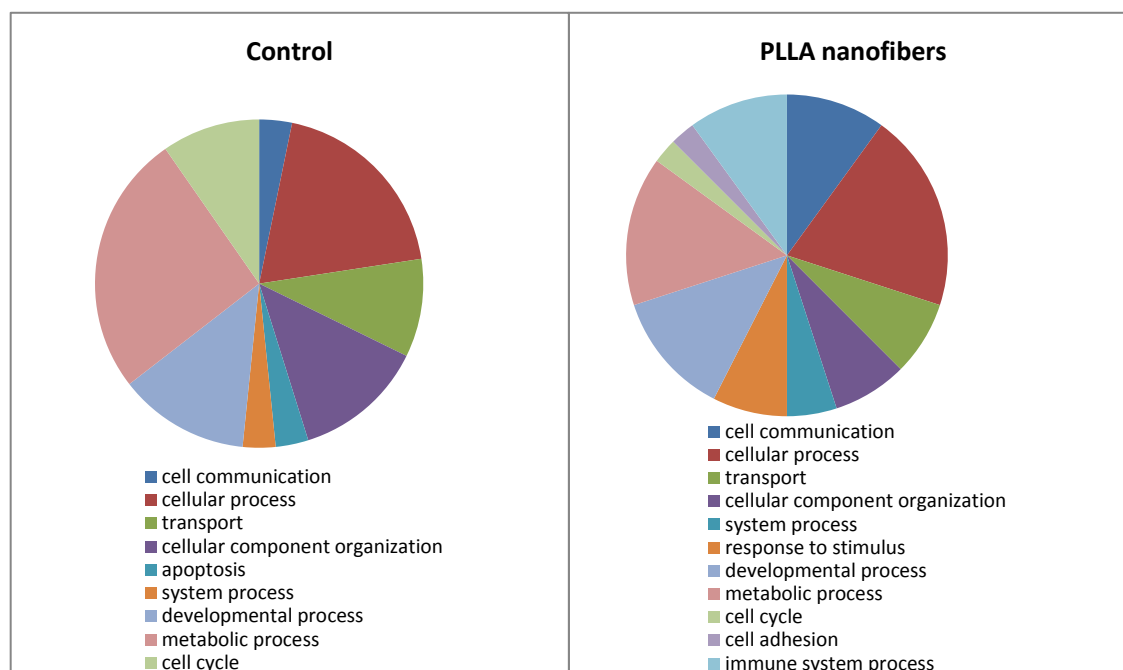
Figure 19 - Biological processes in which the altered proteins are involved. The percentage is based on the number of proteins that are classified into the referred biological process. According to PANTHER gene list.

The analysis of figure 16 indicates that protein expression changes upon culture on PLLA nanofibers. Overall, PLLA nanofibers seem to favor the expression of proteins involved in cell adhesion while downregulating proteins involved in cell metabolism. Since various functions have been attributed to some of these proteins, a more detailed analysis was performed, in which the molecular mechanisms in which those proteins are involved were considered (figure 20).
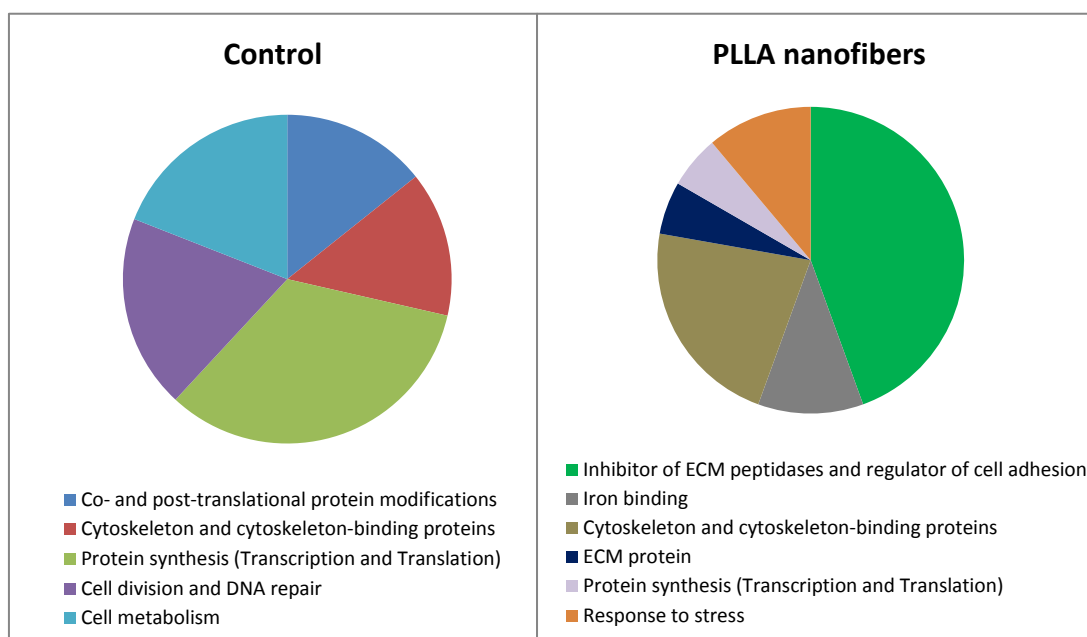
Figure 20 – Cellular mechanisms in which the identified proteins are involved. Control: unique and upregulated in SH-SY5Y cells cultured on culture dish; PLLA nanofibers: unique and upregulated in SH-SY5Y cells cultured on PLLA nanofibers.

Comparing both pie charts, relevant differences between both conditions arise. Altered proteins identified in control conditions are mainly involved in cellular processes required for cellular proliferation: protein synthesis and protein modifications (necessary for cell growth), and cell division. On the other hand, proteins only identified or upregulated in the cells grown on PLLA nanofibers are mainly involved the regulation of ECM stability and in the regulation of cell cytoskeleton, suggesting that cells grown on PLLA nanofibers upregulate proteins that allow them to adapt to the substrate. Table 11 depicts the mass spec data of three proteins relevant for cells to cytoskeleton and ECM remodeling, and the levels of PARP that was also found altered.

Table 11 - Proteins whose levels were highly altered in SH-SY5Y cells cultured on PLLA nanofibers (NFs). '*N*', nanofibers condition; '*C*', control conditions; '*1*' and '*2*',

	Protein name	Sample	Mascot Score	emPAI	Normalized emPAI	Variation	Function
Unique in NFs	Kininogen-1	N1	41	0,06	1,3636	Unique	Extracellular cysteine proteinase inhibitor
		N2	48	0,06	1,2422		
	Vitronectin	N1	102	0,08	1,8182	Unique	Cell adhesion molecule
		N2	124	0,08	1,6563		
Upregulated in NFs	Gelsolin	C1	84	0,05	0,4227	5x	Actin binding
		C2	73	0,05	0,5187		
		N1	76	0,11	2,3109		
		N2	200	0,22	2,6862		
Upregulated in control	PARP1	C1	193	0,17	5,4839	0.5x	Transcription regulator / DNA repair
		C2	288	0,27	5,9603		
		N1	77	0,08	4,7619		
		N2	34	0,04	0,9877		

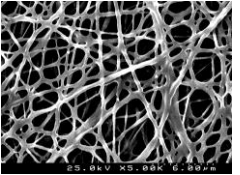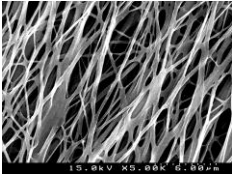As depicted in table 11, SH-SY5Y cells grown on PLLA nanofibers increases the levels of proteins involved in actin remodeling, such as gelsolin (5 times higher levels) and proteins of the ECM - vitronectin or that promote its stability – kininogen-1. On the other hand PARP in its full length is a protein involved in the DNA repair that seems to be downregulated (by 50%) upon culture with PLLA nanofibers.

5. Discussion

This work aimed to address the ability of non-polarized and polarized PLLA samples to potentiate neuronal differentiation, in view of their potential use in regenerative medicine. For that, different cellular responses upon culture on these materials were evaluated, including: cell adhesion, cell viability and proliferation, cell morphology and differentiation. Results are summarized in table 12.

Table 12 – Main findings of the evaluated cellular responses upon culture on the different PLLA samples. (0) non-polarized polymers, (-) negatively polarized, (+) positively polarized; arrows indicate increases or decreases over the control; SF – stress fibers, AD – Actin depolymerization; N/A – non-applicable; $_\phi$ - not found.

		PLLA films			PLLA random nanofibers			PLLA aligned nanofibers		
		(0)	**(-)**	**(+)**	**(0)**	**(-)**	**(+)**	**(0)**	**(-)**	**(+)**
SEM micrographs										
Adhesion		No measurable alterations								
Viability		↓↓	↓	↓	↓↓	↓	↓	≈	≈	≈
Morphology & Distribution		Cuboid	Cuboid and Spread	Cuboid Spread	Round Aggreg.	Round Very Aggreg.	Round Very Aggreg.	Cuboid/ round Spread	Round Very Aggreg.	Round Aggreg. / Spread
Cytoskeleton	SF	≈	≈	≈		φ			φ	
Cytoskeleton	AD	≈/↑	≈	≈	↑	↑↑	↑↑	↑	↑↑	↑↑
Neuron - like differentiation		N/A			↑	↑	↑	↑	↑	↑↑
Neuritic outgrowth		N/A			N/A			↑	↑↑	↑↑

5.1 Non-polarized PLLA samples: influence of topography on cellular behavior

In their natural 3D environment, cells are subjected to different sources of stimuli: biochemical signals such as growth factors and cytokines; ECM architecture that comprises its composition, density and alignment; and external mechanical properties, such as matrix stiffness[2] and external forces. Thus, the mechanical properties of the substrate on which the cells are cultured play an important role in controlling cellular activity, including cell proliferation and cell differentiation in embryogenesis and in regenerative conditions. In order to understand the cellular responses obtained upon cell culture on the different PLLA samples, it is important to address the mechanical forces acting on cells. The overall functional force of the cell is provided by intracellular, contractile, force-generating motor proteins such as myosin; by the cytoskeleton; and by cell adhesion to the substrate (via integrins) and to other cells (via cadherins) [84, 85].

Relatively to adhesion, apparently the PLLA samples produced no substantial differences in the number of SH-SY5Y adherent cells after 2h of culture (figure 9). Not even coating with laminin, a natural extracellular matrix protein, improved the adherence of SH-SY5Y cells, what could be explained by the natural high adhesiveness property of these cells. Even though there are no measurable alterations in the number of adherent cells, PLLA samples are most probably affecting the quality of those adhesions, by altering the size and strength of focal adhesions (FAs). As mentioned before, FAs are important cellular adhesion structures that provide a physical link between the intracellular actin cytoskeleton and the ECM, and transduces force between the cell and its microenvironment [86]. This inside-out communication between the cell and its substrate alters cellular adhesion, being believed that this communication causes different cellular adhesion in 2D or 3D cultures [87]. Provenzano and colleagues described that the assembly of 3D-matrix adhesions are decreased due to disruption of myosin-based contractility mechanisms or the actin cytoskeleton itself, which releases the intracellular tension [88]. We postulate that, upon culture on PLLA films, a flat rigid substrate, more force is transmitted through the actin cytoskeleton and therefore, more FA is assembled. On the other hand, upon culture on PLLA nanofibers, a porous and less stiff substrate, less intracellular force is probably generated, and therefore, less FA is assembled. To further evaluate this, FA could be marked using FAK, one of its resident kinases, and its number scored under the microscope.

---

[2] Stiffness of an elastic material is the internal resistance to deformation produced by the application of force. It is a structural property (also known as an extensive property) because it depends on the size, organization and shape of the material.

Besides promoting adhesion, a good scaffold for neuronal regeneration should be biocompatible with the host tissue and produce a low cytotoxic response. We thus tested cell proliferation upon culture on PLLA samples, and differences became evident (figure 10). Although PLLA samples do not induce cytotoxicity below cell plating number, in general, they decrease or decelerate cell proliferation, with this effect being potentiated by coating with laminin. Laminin coating by itself reduces the number of metabolic-active cells in culture, in comparison to uncoated control. Therefore, PLLA films and random nanofibers behave like ECM mimetic scaffolds. PLLA aligned nanofibers, on the other hand, do not seem to affect the number of metabolic-active cells.

Two main hypotheses could explain the decrease in the number of viable cells seen for PLLA films and random nanofibers: an increase in cell apoptosis or an inhibition of cell proliferation. To test for cell apoptosis, cleaved PARP levels were quantified. PARP is a protein cleaved by caspase 3 and 7 when apoptosis is induced by an external or intrinsic factor. According to our Western blot analysis, PLLA films and nanofibers decrease cleaved PARP levels, being this particularly evident for random nanofibers (figure 11). However, when performing our proteomic analysis (table 11), we noticed that the levels of full length PARP also seem to decrease (by 50%) when SH-SY5Y cells are cultured on PLLA random nanofibers. This might indicate that the observed decrease of cleaved PARP levels is due to a decrease of full length PARP itself. As PARP is a DNA-repair protein required for cell division, the decrease in the number of viable cells is probably due to inhibition of cell proliferation (second hypothesis) and not due to an increase in cell apoptosis. Furthermore, we observed that other proteins involved in cell cycle and cell metabolism are diminished for the PLLA nanofibers. Thus, when SH-SY5Y cells are cultured on the random nanofibrous substrate, their proliferation is most probably inhibited. This effect might also be induced by PLLA films, which presented similar decreases in bands (Ponceau S staining) containing cell cycle-related proteins.

Although further replicas are required to validate the differences of specific protein content by mass spec analysis of cells grown on PLLA nanofibers (in addition to the analysis of PLLA films and aligned nanofibers), our results on decreased cell proliferation are in agreement with the literature. Several studies have addressed the role of substrate stiffness in cell proliferation and cell differentiation, suggesting that differences in substrate stiffness are "sensed" in focal adhesions and transmitted to the cell nucleus, influencing transcription and cell proliferation regulatory machineries [84, 89, 90]. Although this could be initially seen as an

adverse effect, various studies suggest that differentiation is normally associated with reduced cell proliferation [52].

Hence, our next step was to assess SHSY-5Y cell differentiation by studying their morphological alterations upon culture on PLLA samples. Even though all the cytoskeleton elements contribute to the mechanical properties of cells, the actin cytoskeleton is the most dynamic and "force-responsive" structure [91]. Thus, F-actin was stained in order to address the effects of PLLA samples on cell morphology and cytoskeleton remodeling (figure 12).

Coating with laminin does not greatly affect cell shape and the overall cell morphology; however it produces alterations on the actin cytoskeleton polymerization state. Firstly, it is observable a decrease in the organization of F-actin into stress fibers, and an increase of F-actin depolymerization. Further, actin and β-tubulin levels decrease when laminin coating is performed (figure 13). Indeed, a recent study, which evaluated the role of laminin in neuritic outgrowth, revealed laminin as one of the most significant cues to FAK activation, which leads to morphological changes through multiple signal transduction events [92].

Besides affecting SH-SY5Y cell proliferation, PLLA samples also change cell morphology. In general, PLLA films cause fewer alterations in cell morphology, what is in accordance to the less dramatic alterations detected in actin and β-tubulin levels quantification (figure 13). On the other hand, PLLA nanofibers simultaneously decrease tubulin levels, completely alter SH-SY5Y cell morphology, and induce the most accentuated decrease on actin levels (figures 12 and 13). These differential effects might be attributed to the differences in films and nanofibers substrate rigidity. On PLLA films or on culture dish, cells may generate stronger tractional forces to the substrate components and activate RhoA signaling. RhoA, a GTPase protein that regulates actin polymerization into stress fibers, activates ROCK, a kinase that increases actomyosin contractility and actin stabilization [91]. These events promote the development of focal adhesions and stress fibers, visible upon F-actin staining of cells grown on dishes and still visible in various cells grown on PLLA films. In contrast, PLLA nanofibers' softer substrate might in fact highly disrupt the myosin-based contractility mechanisms and the actin cytoskeleton, as described by Provenzano and colleagues, and thus no stress fibers are visible. When aligned, nanofibers partially maintain cells morphology and do not decrease significantly beta-tubulin, while similarly inducing F-actin depolymerization and reducing actin by 45% (figures 12 and 13). Hence, it appears that when in meshes, the pores of the nanofibers substrate induce a change of cuboid to a round morphology, in a process where the 'neurite-like' projections and their beta-tubulin component are lost/decreased.

This disruption of actin cytoskeleton may be achieved through actin-binding proteins such as gelsolin, whose levels were found increased according to the proteomic analysis of SH-SY5Y cells cultured on PLLA nanofibers (table 11). Actin binding proteins are important regulators of actin polymerization at focal adhesions, and are crucial for mechanosensing. Gelsolin is regulated by Ca^{2+} and modifies the length of F-actin by severing pre-existing actin filaments and capping the fast growing barbed end of actin filaments [93]. Recently, it has been suggested that stretch-activated cation channels cause an additional Ca^{2+} influx that will cause actin reorganization [94]. Therefore, gelsolin might be activated upon cell culture on PLLA nanofibers due to substrate-induced membrane stretching, and act as a crucial effector protein in the transduction of mechanical signals (at focal adhesions) to the cytoskeleton, leading to the visible increase in actin depolymerization.

Additionally, our proteomic analysis revealed that SH-SY5Y cells might be producing new extracellular matrix, since it increases levels of the ECM protein vitronectin, and also inhibit its degradation, as many inhibitors of ECM degradation are found upregulated (figure 20, table 11). Therefore, besides the negative effect on cell proliferation, cells cultured on PLLA nanofibers seem to be actively altering its extracellular environment, what has been described as an effect of integrin signaling, to reveal or disrupt integrin-binding sites [95, 96].

Until now, it is evident that the different PLLA samples produce alterations in cell proliferation, cell shape and cytoskeleton dynamics. Moreover, these alterations mimic some of the laminin properties, suggesting an ECM-like behavior. As mentioned before, topographical characteristics of the scaffolds determine the orientation of biological molecules adsorption onto the substrate, regulating characteristics of cells such as cell morphology [40]. Comparing substrate topographies of PLLA films and nanofibers, it is plausible that PLLA nanofibers will be more suited for a neuronal regenerative approach (see figure 21). Besides their porous structure configuration, permitting a better three-dimensional support for cells, their softness better mimics the brain tissue and thus should potentiate neurite branching [97]. Furthermore, unpublished results from our laboratory revealed that at the most earlier stages of neuronal-like and neuronal differentiation, actin and tubulin levels first decrease; these data strengthens the highest nanofibers' potential for facilitating differentiation, when compared to films. Thus, our next step was to analyze the neuron-like differentiation of SH-SH5Y cells cultured on PLLA random and aligned nanofibers by using the morphogen retinoic acid.

As we expected, our results indicate that neuron-like differentiation is more accentuated when cells are cultured on PLLA nanofibers in comparison to cells cultured on the culture dish

(figure 16). Furthermore, aligned PLLA nanofibers seem to increase neurite length in SH-SY5Y cells, an effect also visible in embryonic cortical neurons, although non-statistically different (figure 17).

In synthesis, our results agree with Yang and colleagues' data, which shown that PLLA aligned nanofibers induce an increase in neurite length of differentiated neural stem cells, over random nanofibers. Consequently, PLLA aligned nanofibers would be more appropriated for an axotomy regenerative approach, where the extension of the growth is desired. Figure 21 summarizes and represents the main cellular responses upon culture with PLLA nanofibers.
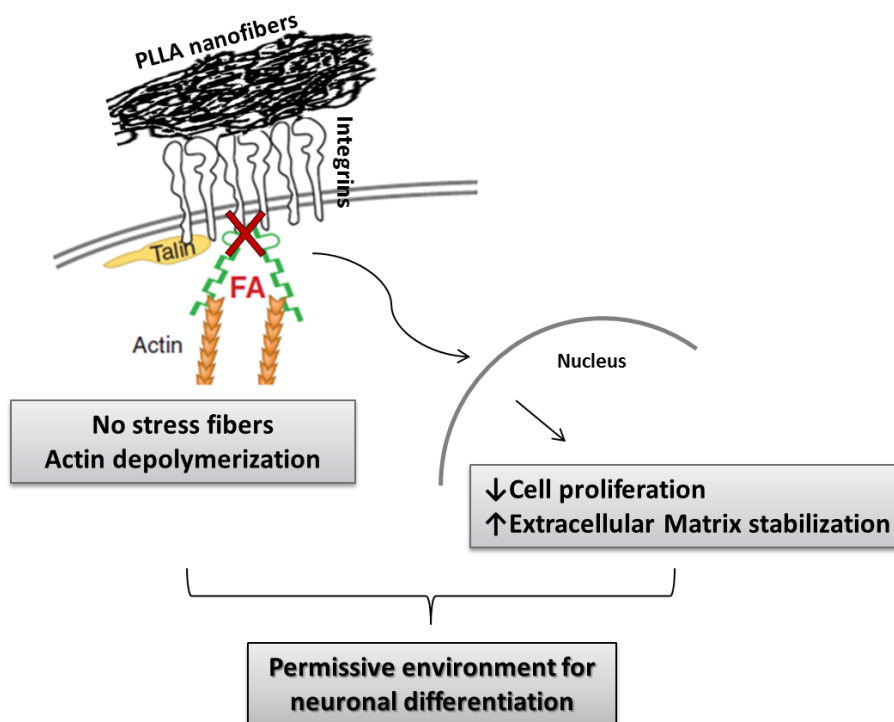
Figure 21 – SH-SY5Y cellular responses upon culture with PLLA nanofibers. FA – focal adhesion.

5.2   Polarized PLLA samples: influence of polarization on neuritic outgrowth

Besides the effects of the scaffold's mechanical properties on cellular activity, we also aimed to test if polarization of PLLA samples might potentiate neuronal differentiation. As mentioned before, PLLA samples can be polarized by the application of an external electric field, thus generating negatively and positively polarized surfaces.

Concerning cellular proliferation, it is visible that polarization, either negative or positive, diminishes the proliferation rate in the initial cell growth phases for polarized PLLA films and

random nanofibers (figure 10). Of note, coating does not increase (and even slightly decrease) this effect in polarized polymers. Nonetheless, after 11 days in culture, the number of viable cells cultured on these substrates coincides with the ones in uncoated and coated controls. Therefore, polarization of PLLA films and random nanofibers seem to have less detrimental effect on cell proliferation at a long-term (11 days). Polarization of PLLA aligned nanofibers does not change significantly the number of viable cells relatively to control, what was also observed in their non-polarized counterparts. These results are in agreement to the idea that electrical stimulation initiates molecular signaling of survival, since polarization reverts the decrease in cell proliferation observed in PLLA films and random nanofibers, although only in the last days of culture [76]. Furthermore, unpublished results on osteoblast-like cells show an increase in cell proliferation upon culture with polarized PLLA films.

Polarization by itself affects SH-SY5Y cell morphology and cell distribution on the substrate. Noticeably, at this time point (11 days), it is also observed that the number of fixed cells represents what is detected on the viability assay: approximately the same number of cells compared to the control (figure 12). Furthermore, the analysis of F-actin staining of SH-SY5Y cells cultured on polarized PLLA films indicates higher cell spreading and cell elongation than non-polarized films, suggesting an increase in cell-substrate adhesion. However, both negatively and positively polarized PLLA nanofibers (random or aligned) seem to increase cell-cell adhesion, creating dense cell agglomerates, as if the cell-substrate adhesion is prevented. Coating and nanofibers alignment partially revert these effects. Nevertheless, further studies are required to confirm that this effect on cell aggregation is not due to other factors besides polarization.

Concerning cytoskeleton alterations, it is observed that negatively and positively polarized films revert the partial induction of F-actin depolymerization by their non-polarized counterpart. This effect is confirmed by the increase in actin and β-tubulin levels over the non-polarized sample. Polarization of PLLA random nanofibers, on the other hand maintains actin distribution and depolymerization, and only slightly increases actin levels, while inducing a higher increase in β-tubulin. Polarization of PLLA aligned nanofibers almost does not induce major alterations in actin and β-tubulin levels (figure 14 and 15).

In conclusion, better morphological outputs, more elongation and cell substrate-adhesion on films, and more cell spreading on nanofibers are obtained when polarized PLLA samples are coated with laminin, in comparison to their coated non-polarized counterparts. This effect might be attributed to a better laminin adsorption in the poled zones of PLLA samples. Indeed, Barroca and colleagues revealed that there is a higher concentration of adsorbed proteins (fibronectin) on

polarized areas of PLLA films [98]. This property of polarized PLLA polymer might also favor the adsorption of adhesive proteins to the substrate and thus potentiate neuronal differentiation.

To evaluate if polarization also potentiates neuronal differentiation, two assays were performed: neuron-like differentiation, where SH-SY5Y cells were grown on PLLA nanofibers and incubated with RA, and culture of embryonic cortical neurons on PLLA aligned nanofibers. Polarization of PLLA nanofibers (random and aligned) seems to increase the length of neurites after 2 days in culture (figure 16). Furthermore, culture on positively polarized aligned nanofibers seems to enhance this effect for RA-induced differentiating SH-SY5Y neuronal-like cells.

Regarding neuronal differentiation (figure 17), while non-polarized PLLA aligned nanofibers lead to a slight increase in neurite length of cultured embryonic cortical neurons, this effect is significantly increased by polarization.

Polarization of PLLA samples was performed by electrical induction in order to align its dipoles, and thus enhancing the intrinsic piezoelectric property of PLLA. Thus cells cultured on these polarized samples might be subjected to some degree of electrical stimulation, generated either due to alterations on cell surface charges or activation of piezoelectric effect due to cell attachment and migration. Electrical activity is known to promote neuroprotection and neuronal differentiation. Our results of embryonic culture on polarized PLLA aligned nanofibers clearly show that, in addition to the effect of fiber orientation, polarization increases the neurite length of cortical neurons. One of the acceptable explanations for this effect is that depolarization of neuron results in the opening of voltage-gated ion channels that increase intracellular calcium levels. Calcium is a strong regulator of growth cone responses as it modulates the state of polymerization of actin filaments and microtubules [5, 18]. Furthermore, the electrophoretic redistribution of surface receptors and consequent influx of Ca^{2+} is rather local than global, as it seems to be inducing a directing effect of neurite elongation. Nevertheless, further studies are required to determine the exact cellular response to polarization of PLLA samples.

6. Concluding remarks

In conclusion, all PLLA samples meet the biocompatibility criterion, as they allow cells to grow (although at a lower rate) and do not increase apoptosis. Concerning the functionality criteria, the highly porous PLLA nanofibers' substrate seems to induce dramatic cytoskeletal alterations that, upon an extracellular cue (RA), might potentiate the neuron-like differentiation. Furthermore, when PLLA nanofibers are aligned, longer neurites seem to be induced. Lastly, the biocompatibility and functionality criteria seem to be enhanced when PLLA polymers are polarized, since there is a reversion of the decrease in cell proliferation observed on non-polarized polymers, as well as an enhancement of neuritic outgrowth.

This study has not only confirmed the effectiveness of PLLA-based materials for neuronal differentiation, but also suggests the potential of its polarization to facilitate this process, in view of a neuronal regenerative approach. Nevertheless, future experiments should clarify the decrease in cell proliferation and address the cellular adhesion to these PLLA samples.

7. References

1.   Ross MH, Pawlina W. HISTOLOGY A Text and Atlas. 6 ed. Philadelphia: Lippincott Williams & Wilkins; 2011.

2.   Purves D, Augustine GJ, Fitzpatrick D, Hall WC, Lamantia A-S, Mcnamara JO, Williams SM. Neuroscience 3ed. Sunderland, Massachusetts U.S.A.: Sinauer Associates, Inc; 2004

3.   Hotulainen P, Hoogenraad CC. Actin in dendritic spines: connecting dynamics to function. The Journal of cell biology. 2010;189(4):619-29.

4.   Fitch MT, Silver J. CNS injury, glial scars, and inflammation: Inhibitory extracellular matrices and regeneration failure. Exp Neurol. 2008;209(2):294-301.

5.   Mattson MP. Establishment and Plasticity of Neuronal Polarity. Journal of Neuroscience Research. 1999;57:577–89.

6.   Whitford KL, Dijkhuizen P, Polleux F, Ghosh A. Molecular control of cortical dendrite development. Annu Rev Neurosci. 2002;25:127-49.

7.   Rossi F, Gianola S, Corvetti L. Regulation of intrinsic neuronal properties for axon growth and regeneration. Prog Neurobiol. 2007;81(1):1-28.

8.   Polleux F, Snider W. Initiating and growing an axon. Cold Spring Harb Perspect Biol. 2010;2(4):a001925.

9.   Hirokawa N, Takemura R. Molecular motors and mechanisms of directional transport in neurons. Nature Reviews Neuroscience. 2005;6(3):201-14.

10.   Gallo G, Lanier LM. Neurobiology of Actin: From Neurulation to Synaptic Function. New York: Springer; 2011.

11.   Siegel G, Agranoff B, Albers R, et al. Basic Neurochemistry: Molecular, Cellular and Medical Aspects. 6 ed. Philadelphia: Lippincott-Raven; 1999.

12.   Conde C, Caceres A. Microtubule assembly, organization and dynamics in axons and dendrites. Nature reviews Neuroscience. 2009;10(5):319-32.

13.   Lee SH, Dominguez R. Regulation of actin cytoskeleton dynamics in cells. Molecules and cells. 2010.

14.   da Silva JS, Dotti CG. Breaking the neuronal sphere: regulation of the actin cytoskeleton in neuritogenesis. Nature reviews Neuroscience. 2002;3(9):694-704.

15.   Witte H, Bradke F. The role of the cytoskeleton during neuronal polarization. Current opinion in neurobiology. 2008;18(5):479-87.

16.   Yao L, Pandit A, Yao S, McCaig CD. Electric field-guided neuron migration: a novel approach in neurogenesis. Tissue Eng Part B Rev. 2011;17(3):143-53.

17.   Lowery LA, Vactor DV. The trip of the tip: Understanding the growth cone machinery. Nature Reviews Molecular Cell Biology. 2009;10(5):332-43.

18.   Henley J, Poo MM. Guiding neuronal growth cones using Ca2+ signals. Trends in cell biology. 2004;14(6):320-30.

19. Flynn KC, Pak CW, Shaw AE, Bradke F, Bamburg JR. Growth cone-like waves transport actin and promote axonogenesis and neurite branching. Developmental neurobiology. 2009;69(12):761-79.

20. Gertz CC, Leach MK, Birrell LK, Martin DC, Feldman EL, Corey JM. Accelerated neuritogenesis and maturation of primary spinal motor neurons in response to nanofibers. Developmental neurobiology. 2010;70(8):589-603.

21. Ciobanasu C, Faivre B, Le Clainche C. Actin dynamics associated with focal adhesions. International journal of cell biology. 2012;2012:941292.

22. CLAINCHE CL, CARLIER M-F. Regulation of Actin Assembly Associated With Protrusion and Adhesion in Cell Migration. Physiol Rev. 2008;88:489-513.

23. Curtis Id. Intracellular Mechanisms for Neuritogenesis. Italy: Springer Science+Business Media, LLC; 2007.

24. Harburger DS, Calderwood DA. Integrin signalling at a glance. J Cell Sci. 2009;122(Pt 2):159-63. doi: 10.1242/jcs.018093.

25. Wu X, Reddy DS. Integrins as receptor targets for neurological disorders. Pharmacology and Therapeutics. 2012;134(1):68-81.

26. Zhou FQ, Snider WD. Intracellular control of developmental and regenerative axon growth. Philosophical Transactions of the Royal Society B: Biological Sciences. 2006;361(1473):1575-92.

27. de Miguel FF, Vargas J. Native extracellular matrix induces a well-organized bipolar outgrowth pattern with neurite extension and retraction in cultured neurons. The Journal of Comparative Neurology. 2000;417(4):387-98.

28. Liu K, Tedeschi A, Park KK, He Z. Neuronal intrinsic mechanisms of axon regeneration. Annu Rev Neurosci. 2011;34:131-52.

29. Park KK, Liu K, Hu Y, Smith PD, Wang C, Cai B, Xu B, Connolly L, Kramvis I, Sahin M, He Z. Promoting Axon Regeneration in the Adult CNS by Modulation of the PTEN/mTOR Pathway. Science. 2008;322(5903):963-6.

30. Franz S, Weidner N, Blesch A. Gene therapy approaches to enhancing plasticity and regeneration after spinal cord injury. Exp Neurol. 2012;235(1):62-9.

31. Bloom OE, Morgan JR. Membrane trafficking events underlying axon repair, growth, and regeneration. Molecular and cellular neurosciences. 2011;48(4):339-48.

32. Seil JT, Webster TJ. Electrically active nanomaterials as improved neural tissue regeneration scaffolds. Wiley Interdiscip Rev Nanomed Nanobiotechnol. 2010;2(6):635-47.

33. WFawcett J, Asher RA. The glial scar and central nervous system repair. Brain Research Bulletin. 1999;49(6):377–91.

34. Wang M, Zhai P, Chen X, Schreyer DJ, Sun X, Cui F. Bioengineered scaffolds for spinal cord repair. Tissue Eng Part B Rev. 2011;17(3):177-94.

35. Vargas ME, Barres BA. Why is Wallerian degeneration in the CNS so slow? Annu Rev Neurosci. 2007;30:153-79.

36. Cunha C, Panseri S, Antonini S. Emerging nanotechnology approaches in tissue engineering for peripheral nerve regeneration. Nanomedicine. 2011;7(1):50-9.

37. Re F, Gregori M, Masserini M. Nanotechnology for neurodegenerative disorders. Maturitas. 2012.

38. Forraz N, Wright K, Jurga M, McGuckin C. Experimental therapies for repair of the central nervous system: stem cells and tissue engineering. J Tissue Eng Regen Med. 2012.

39. Guo B, Sun Y, Finne-Wistrand A, Mustafa K, Albertsson AC. Electroactive porous tubular scaffolds with degradability and non-cytotoxicity for neural tissue regeneration. Acta Biomater. 2012;8(1):144-53.

40. He L, Liao S, Quan D, Ma K, Chan C, Ramakrishna S, Lu J. Synergistic effects of electrospun PLLA fiber dimension and pattern on neonatal mouse cerebellum C17.2 stem cells. Acta Biomater. 2010;6(8):2960-9.

41. Gilmore JL, Yi X, Quan L, Kabanov AV. Novel nanomaterials for clinical neuroscience. J Neuroimmune Pharmacol. 2008;3(2):83-94.

42. Pancrazio JJ. Neural interfaces at the nanoscale. Nanomedicine. 2008;3(6):823-30.

43. Modi G, Pillay V, Choonara YE, Ndesendo VM, du Toit LC, Naidoo D. Nanotechnological applications for the treatment of neurodegenerative disorders. Prog Neurobiol. 2009;88(4):272-85.

44. Lin N, Huang J, Dufresne A. Preparation, properties and applications of polysaccharide nanocrystals in advanced functional nanomaterials: a review. Nanoscale. 2012;4(11):3274-94.

45. Silva GA. Neuroscience nanotechnology: progress, opportunities and challenges. Nature reviews Neuroscience. 2006;7(1):65-74.

46. Suh WH, Suslick KS, Stucky GD, Suh YH. Nanotechnology, nanotoxicology, and neuroscience. Prog Neurobiol. 2009;87(3):133-70.

47. Seidlits SK, Lee JY, Schmidt CE. Nanostructured scaffolds for neural applications. Nanomedicine 2008;3(2):183-99.

48. Lamour G, Eftekhari-Bafrooei A, Borguet E, Soues S, Hamraoui A. Neuronal adhesion and differentiation driven by nanoscale surface free-energy gradients. Biomaterials. 2010;31(14):3762-71.

49. Gupta D, Venugopal J, Prabhakaran MP, Dev VR, Low S, Choon AT, Ramakrishna S. Aligned and random nanofibrous substrate for the in vitro culture of Schwann cells for neural tissue engineering. Acta Biomater. 2009;5(7):2560-9.

50. Lee Y-S, Livingston Arinzeh T. Electrospun Nanofibrous Materials for Neural Tissue Engineering. Polymers. 2011;3(1):413-26.

51. Wen X, Tresco PA. Effect of filament diameter and extracellular matrix molecule precoating on neurite outgrowth and Schwann cell behavior on multifilament entubulation bridging device in vitro. Journal of Biomedical Materials Research Part A. 2006;76A(3):626-37.

52. Badami AS, Kreke MR, Thompson MS, Riffle JS, Goldstein AS. Effect of fiber diameter on spreading, proliferation, and differentiation of osteoblastic cells on electrospun poly(lactic acid) substrates. Biomaterials. 2006;27(4):596-606. Epub 2005 Jul 15.

53. Mahairaki V, Lim SH, Christopherson GT, Xu L, Nasonkin I, Yu C, Mao HQ, Koliatsos VE. Nanofiber matrices promote the neuronal differentiation of human embryonic stem cell-derived neural precursors in vitro. Tissue Eng Part A. 2011;17(5-6):855-63. doi: 10.1089/ten.TEA.2010.0377. Epub 2010 Dec 18.

54. Kabiri M, Soleimani M, Shabani I, Futrega K, Ghaemi N, Ahvaz HH, Elahi E, Doran MR. Neural differentiation of mouse embryonic stem cells on conductive nanofiber scaffolds. Biotechnol Lett. 2012;34(7):1357-65.

55. Timnak A, Gharebaghi FY, Shariati RP, Bahrami SH, Javadian S, Emami Sh H, Shokrgozar MA. Fabrication of nano-structured electrospun collagen scaffold intended for nerve tissue engineering. J Mater Sci Mater Med. 2011;22(6):1555-67.

56. Fuhrmann T, Hillen LM, Montzka K, Woltje M, Brook GA. Cell-cell interactions of human neural progenitor-derived astrocytes within a microstructured 3D-scaffold. Biomaterials. 2010;31(30):7705-15.

57. Gros T, Sakamoto JS, Blesch A, Havton LA, Tuszynski MH. Regeneration of long-tract axons through sites of spinal cord injury using templated agarose scaffolds. Biomaterials. 2010;31(26):6719-29.

58. Daud MF, Pawar KC, Claeyssens F, Ryan AJ, Haycock JW. An aligned 3D neuronal-glial co-culture model for peripheral nerve studies. Biomaterials. 2012;33(25):5901-13.

59. Bechara S, Wadman L, Popat KC. Electroconductive polymeric nanowire templates facilitates in vitro C17.2 neural stem cell line adhesion, proliferation and differentiation. Acta Biomater. 2011;7(7):2892-901.

60. Sun M, McGowan M, Kingham PJ, Terenghi G, Downes S. Novel thin-walled nerve conduit with microgrooved surface patterns for enhanced peripheral nerve repair. J Mater Sci Mater Med. 2010;21(10):2765-74.

61. Bhang SH, Jeong SI, Lee TJ, Jun I, Lee YB, Kim BS, Shin H. Electroactive electrospun polyaniline/poly[(L-lactide)-co-(epsilon-caprolactone)] fibers for control of neural cell function. Macromol Biosci. 2012;12(3):402-11.

62. Yang F, Murugan R, Ramakrishna S, Wang X, Ma YX, Wang S. Fabrication of nano-structured porous PLLA scaffold intended for nerve tissue engineering. Biomaterials. 2004;25(10):1891-900.

63. Corey JM, Gertz CC, Wang BS, Birrell LK, Johnson SL, Martin DC, Feldman EL. The design of electrospun PLLA nanofiber scaffolds compatible with serum-free growth of primary motor and sensory neurons. Acta Biomater. 2008;4(4):863-75.

64. Lam HJ, Patel S, Wang A, Chu J, Li S. In vitro regulation of neural differentiation and axon growth by growth factors and bioactive nanofibers. Tissue engineering Part A. 2010;16(8):2641-8.

65. Yang F, Murugan R, Wang S, Ramakrishna S. Electrospinning of nanomicro scale poly(l-lacticacid) aligned fibers and their potential in neural tissue engineering. Biomaterials. 2005;26(15):2603-10.

66. Xiong Y, Zeng YS, Zeng CG, Du BL, He LM, Quan DP, Zhang W, Wang JM, Wu JL, Li Y, Li J. Synaptic transmission of neural stem cells seeded in 3-dimensional PLGA scaffolds. Biomaterials. 2009;30(22):3711-22.

67. Jiang X, Cao HQ, Shi LY, Ng SY, Stanton LW, Chew SY. Nanofiber topography and sustained biochemical signaling enhance human mesenchymal stem cell neural commitment. Acta Biomater. 2012;8(3):1290-302.

68. Koh HS, Yong T, Chan CK, Ramakrishna S. Enhancement of neurite outgrowth using nano-structured scaffolds coupled with laminin. Biomaterials. 2008;29(26):3574-82. doi: 10.1016/j.biomaterials.2008.05.014. Epub Jun 3.

69. Ghaedi M, Soleimani M, Shabani I, Duan Y, Lotfi AS. Hepatic differentiation from human mesenchymal stem cells on a novel nanofiber scaffold. Cell Mol Biol Lett. 2012;17(1):89-106.

70. Hu J, Sun X, Ma H, Xie C, Chen YE, Ma PX. Porous nanofibrous PLLA scaffolds for vascular tissue engineering. Biomaterials. 2010;31(31):7971-7.

71. Schofer MD, Roessler PP, Schaefer J, Theisen C, Schlimme S, Heverhagen JT, Voelker M, Dersch R, Agarwal S, Fuchs-Winkelmann S, Paletta JR. Electrospun PLLA nanofiber scaffolds and their use in combination with BMP-2 for reconstruction of bone defects. PLoS One. 2011;6(9):e25462. doi: 10.1371/journal.pone.0025462. Epub 2011 Sep 28.

72. Fukada E. History and recent progress in piezoelectric polymers. IEEE Trans Ultrason Ferroelectr Freq Control. 2000;47(6):1277-90. doi: 10.109/58.883516.

73. Guo HF, Li ZS, Dong SW, Chen WJ, Deng L, Wang YF, Ying DJ. Piezoelectric PU/PVDF electrospun scaffolds for wound healing applications. Colloids Surf B Biointerfaces. 2012;96:29-36.

74. Lee YS, Collins G, Arinzeh TL. Neurite extension of primary neurons on electrospun piezoelectric scaffolds. Acta Biomater. 2011;7(11):3877-86.

75. Park SC, Oh SH, Seo TB, Namgung U, Kim JM, Lee JH. Ultrasound-stimulated peripheral nerve regeneration within asymmetrically porous PLGA/Pluronic F127 nerve guide conduit. J Biomed Mater Res B Appl Biomater. 2010;94(2):359-66. doi: 10.1002/jbm.b.31659.

76. Goldberg JL. Role of electrical activity in promoting neural repair. Neurosci Lett. 2012;519(2):134-7.

77. Ding Y, Yan Q, Ruan J-W, Zhang Y-Q, Li W-J, Zhang Y-J, Li Y, Dong H, Zeng Y-S. Electro-acupuncture promotes survival, differentiation of the bone marrow mesenchymal stem cells as well as functional recovery in the spinal cord-transected rats. BMC Neuroscience. 2009;10(1):35.

78. Romero-Calvo I, Ocón B, Martínez-Moya P, Suárez MD, Zarzuelo A, Martínez-Augustin O, de Medina FS. Reversible Ponceau staining as a loading control alternative to actin in Western blots. Analytical Biochemistry. 2010;401(2):318-20.

79. Ishihama Y, Oda Y, Tabata T, Sato T, Nagasu T, Rappsilber J, Mann M. Exponentially Modified Protein Abundance Index (emPAI) for Estimation of Absolute Protein Amount in Proteomics by the Number of Sequenced Peptides per Proteins. Molecular & Cellular Proteomics. 2005;4:1265-72.

80. Boulares AH, Yakovlev AG, Ivanova V, Stoica BA, Wang G, Iyer S, Smulson M. Role of Poly(ADP-ribose) Polymerase (PARP) Cleavage in Apoptosis: CASPASE 3-RESISTANT PARP MUTANT INCREASES RATES OF APOPTOSIS IN TRANSFECTED CELLS. Journal of Biological Chemistry. 1999;274(33):22932-40.

81. Müller T, Concannon CG, Ward MW, Walsh CM, Tirniceriu AL, Tribl F, Kögel D, Prehn JHM, Egensperger R. Modulation of gene expression and cytoskeletal dynamics by the amyloid precursor protein intracellular domain (AICD). Molecular Biology of the Cell. 2007;18(1):201-10.

82. Påhlman S, Ruusala A-I, Abrahamsson L, Mattsson MEK, Esscher T. Retinoic acid-induced differentiation of cultured human neuroblastoma cells: a comparison with phorbolester-induced differentiation. Cell Differentiation. 1984;14(2):135-44.

83. Mi H, Muruganujan A, Thomas PD. PANTHER in 2013: modeling the evolution of gene function, and other gene attributes, in the context of phylogenetic trees. Nucleic Acids Res. 2013;41(Database issue):D377-86. doi: 10.1093/nar/gks118. Epub 2012 Nov 27.

84. Provenzano PP, Keely PJ. Mechanical signaling through the cytoskeleton regulates cell proliferation by coordinated focal adhesion and Rho GTPase signaling. Journal of Cell Science. 2011;124(8):1195-205.

85. Eyckmans J, Boudou T, Yu X, Chen CS. A hitchhiker's guide to mechanobiology. Developmental cell. 2011;21(1):35-47.

86. Geiger B, Bershadsky A, Pankov R, Yamada KM. Transmembrane crosstalk between the extracellular matrix and the cytoskeleton. Molecular Cell Biology 2001;2:793-805.

87. Cukierman E, Pankov R, Stevens DR, Yamada KM. Taking Cell-Matrix Adhesions to the Third Dimension. Science. 2001;294(5547):1708-12.

88. Provenzano PP, Inman DR, Eliceiri KW, Keely PJ. Matrix density-induced mechanoregulation of breast cell phenotype, signaling and gene expression through a FAK-ERK linkage. Oncogene. 2009;28(49):4326-43.

89. Buxboim A, Ivanovska IL, Discher DE. Matrix elasticity, cytoskeletal forces and physics of the nucleus: How deeply do cells 'feel' outside and in? Journal of Cell Science. 2010;123(3):297-308.

90. Moore SW, Sheetz MP. Biophysics of substrate interaction: influence on neural motility, differentiation, and repair. Developmental neurobiology. 2011;71(11):1090-101.

91. Lessey EC, Guilluy C, Burridge K. From Mechanical Force to RhoA Activation. Biochemistry. 2012.

92. Lee JH, Lee HY, Kim HW. Adhesive proteins linked with focal adhesion kinase regulate neurite outgrowth of PC12 cells. Acta Biomater. 2012;8(1):165-72.

93. Chan MW, Arora PD, Bozavikov P, McCulloch CA. FAK, PIP5KIgamma and gelsolin cooperatively mediate force-induced expression of alpha-smooth muscle actin. J Cell Sci. 2009;122(Pt 15):2769-81. doi: 10.1242/jcs.044008. Epub 2009 Jul 13.

94. Titushkin I, Cho M. Regulation of cell cytoskeleton and membrane mechanics by electric field: role of linker proteins. Biophys J. 2009;96(2):717-28. doi: 10.1016/j.bpj.2008.09.035.

95. Boudreau NJ, Jones PL. Extracellular matrix and integrin signalling: the shape of things to come. Biochem J. 1999;339(Pt 3):481-8.

96. Myers J, Santiago-Medina M, Gomez T. Regulation of axonal outgrowth and pathfinding by integrin-ECM interactions. Developmental neurobiology. 2011;71(11):901-23.

97. Flanagan LA, Ju YE, Marg B, Osterfield M, Janmey PA. Neurite branching on deformable substrates. NeuroReport. 2002;13(18):2411-5.

98. Barroca N, Vilarinho PM, Daniel-Da-Silva AL, Wu A, Fernandes MH, Gruverman A. Protein adsorption on piezoelectric poly(L-lactic) acid thin films by scanning probe microscopy. Applied Physics Letters. 2011;98(13).

8. Appendix

Table 13 - Proteins identified through mass spec analysis in SH-SY5Y cells cultured on control and nanofibers (n=2). Protein expression was considered altered if: Mascot score > 32. '*Unique*' - proteins found in both samples of only one condition; '*Upregulated*' - normalized emPAI value is superior in duplicates of the same condition. *(S)* 'Sum' - all the proteins identified in each band, *(T)* '*Total*'- the number of unrepeated proteins.

Band		Proteins with different expression levels							
		Control				**PLLA nanofibers**			
		Unique		**Upregulated**		**Unique**		**Upregulated**	
100 KDa	53	2	Neutral alpha-glucosidase AB	4	ATP-citrate synthase	4	Alpha-2-macroglobulin	0	
					Eukaryotic translation initiation factor 3 subunit B		Complement C3		
			Kinesin-1 heavy chain		Poly [ADP-ribose] polymerase 1		Hemoglobin subunit alpha		
					Transcription intermediary factor 1		Inter-alpha-trypsin inhibitor heavy chain H4		
80 KDa	45	4	Far upstream element-binding protein 2	2	Mitochondrial inner membrane protein	1	Lactotransferrin	3	Gelsolin
			Keratin, type I cytoskeletal 9						Putative heat shock protein HSP 90-beta 4
			Nuclear pore complex protein Nup93		Mannosyl-oligosaccharide glucosidase				Heat shock protein HSP 90-alpha
			Ubiquitin-40S ribosomal protein S27a						
70 KDa	59	2	Dipeptidyl peptidase 3	2	78 kDa glucose-regulated protein	6	Alpha-2-HS-glycoprotein	2	Lactotransferrin
							Hemoglobin subunit alpha		
							Hemoglobin subunit beta		
			Glycine--tRNA ligase		Prelamin-A/C		Keratin, type II cytoskeletal 1		Myristoylated alanine-rich C-kinase substrate
							Kininogen-1		
							Vitronectin		
60 KDa	46	5	Cytoskeleton-associated protein 4	0		1	Lactotransferrin	5	Alpha-2-HS-glycoprotein
			Heterogeneous nuclear ribonucleoprotein R						Heterogeneous nuclear ribonucleoprotein Q
			Prelamin-A/C						Keratin, type I cytoskeletal 9
			Dolichyl-diphosphooligosaccharide--protein glycosyltransferase subunit 1						Keratin, type II cytoskeletal 1
			Ubiquitin-40S ribosomal protein S27a						Kininogen-1
S	203	13		8		12		10	
					43				
T	117				37				

CELL CULTURE SOLUTIONS

- **PBS (1x)**

For a final volume of 500 ml, dissolve one pack of BupH Modified Dulbecco's Phosphate Buffered

Saline Pack (Pierce) in deionised H2O.

Final composition:

- 8 mM Sodium Phosphate

- 2 mM Potassium Phosphate

- 140 mM Sodium Chloride

- 10 mM Potassim Chloride

Sterilize by filtering through a 0.2 µm filter and store at 4ºC.

- **Poly-D-lysine solution**

To a final volume of 10 ml, dissolve in deionised H2O 100 mg of poly-D-lysine (Sigma-Aldrich).

- **10% FBS MEM:F12 (1:1)**

- MEM (Gibco, Invitrogen): 4,805 g

- F12 (Gibco, Invitrogen): 5,315 g

- NaHCO3 (Sigma): 1,5 g

- Sodium pyruvate (Sigma): 0,055 g

- Streptomycin/Penicillin/Amphotericin solution (Gibco, Invitrogen): 10 mL

- 10% FBS (Gibco, Invitrogen): 100 mL

- L-glutamine (200 mM stock solution): 2,5 mL

Dissolve in distilled (d) H_2O;
Adjust the pH to 7.2/ 7.3;
Adjust the volume to 1000 mL with dH_2O.

- **Freezing medium**

- Growth medium (MEM:F12) 7 mL

- FBS (10-20%) 2 mL

- Glycerol (10-15%) or DMSO (5-20%) 1 mL

SDS-PAGE AND IMMUNOBLOTTING SOLUTIONS

- **LGB (Lower gel buffer) (4x)**

To 900 ml of deionised H2O add:

- Tris 181.65 g

- SDS 4 g

Mix until the solutes have dissolved. Adjust the pH to 8.9 and adjust the volume to 1L with deionised H2O.

- **UGB (Upper gel buffer) (5x)**

To 900 ml of deionised H2O add:

- Tris 75.69 g

Mix until the solute has dissolved. Adjust the pH to 6.8 and adjust the volume to 1 L with deionised H2O.

- **30% Acrylamide/0.8% Bisacrylamide**

To 70 ml of deionised H2O add:

- Acrylamide 29.2 g

- Bisacrylamide 0.8 g

Mix until the solute has dissolved. Adjust the volume to 100 ml with deionised water. Filter through a 0.2 µm filter and store at 4oC.

- **10% APS (ammonium persulfate)**

In 10 ml of deionised H2O dissolve 1 g of APS. Note: prepare fresh before use.

- **10% SDS (sodium dodecylsulfate)**

In 10 ml of deionised H2O dissolve 1 g of SDS.

- **Loading Gel Buffer (4x)**

- 1 M Tris solution (pH 6.8) 2.5 mL (250 mM)

- SDS 0.8 g (8%)

- Glicerol 4 ml (40%)

- B-Mercaptoetanol 2 ml (2%)

- Bromofenol blue 1 mg (0.01%)

Adjust the volume to 10 ml with deionised H2O. Store in darkness at room temperature.

- **1 M Tris (pH 6.8) solution**

To 150 ml of deionised H2O add:

- Tris base 30.3 g

Adjust the pH to 6.8 and adjust the final volume to 250 ml.

- **10x Running Buffer**

- Tris 30.3 g (250 mM)

- Glycine 144.2 g (2.5 M)

- SDS 10 g (1%)

Dissolve in deionised H2O, adjust the pH to 8.3 and adjust the volume to 1 L.

- **Resolving (lower) gel solution for gradient gels**

	LGB 5%	LGB 20%
H_2O	17,5 mL	2,2 mL
LGB	7,5 mL	7,5 mL
Acrylamide	5 mL	20 mL
APS	150 µL	150 µL
TEMED	15 µL	15 µL
Total	30 mL	30mL

- **Stacking (upper) gel solution**

	UGB
H_2O	13,2 mL
Acrylamide	2,4 mL
UGB	4 mL
SDS (10%)	200 µL
APS (10%)	200 µL
TEMED	20 µL
Total	30 mL

- **Comassie blue solution**

  For a final volume of 1000 mL add:

Comassie blue (brilliant blue G)	2 g
Methanol	500 mL
Acetic Acid	100 mL
dH_2O	Add until final volume

- **Destaining solution**

  For a final volume of 2000 mL add:

Methanol	500 mL
Acetic Acid	100 mL
dH_2O	Add until final volume

- **1x Transfer Buffer**

- Tris 3.03 g (25 mM)

- Glycine 14.41 g (192 mM)

Mix until solutes dissolution. Adjust the pH to 8.3 with HCl and adjust the volume to 800 ml with deionised H2O. Just prior to use add 200 ml of methanol (20%).

- **10x TBS (Tris buffered saline)**

- Tris 12.11 g (10 mM)

- NaCl 87.66 g (150 mM)

Adjust the pH to 8.0 with HCl and adjust the volume to 1L with deionised H2O.

- **10x TBST (TBS+Tween)**

- Tris 12.11 g (10 mM)

- NaCl 87.66 g (150 mM)

- Tween 20 5 ml (0.05%)

Adjust the pH to 8.0 with HCl and adjust the volume to 1L with deionised H2O.

- **Membranes Stripping Solution** (500 ml)

- Tris-HCl (pH 6.7) 3.76 g (62.5 mM)

- SDS 10 g (2%)

- β-mercaptoethanol 3.5 ml (100 mM)

Dissolve Tris and SDS in deionised H2O and adjust with HCl to pH 6.7. Add the mercaptoethanol and adjust volume to 500 ml.